PANM 2008
Programs and Algorithms of Numerical Mathematics
Dolní Maxov, June 1–6, 2008

Finite Element Modeling of Incompressible Fluid Flows

Pavel Burda, Jaroslav Novotný, Jakub Šístek, Alexandr Damašek

Czech Technical University in Prague
Institute of Thermomechanics CAS

Motivation and goals of the research

- Motivation: Flow in artificial vascular grafts, flow in industrial pipes, flow in glottis
- Qualitative properties of the solution of Navier-Stokes equations near the corners:
  - Asymptotic behaviour of the solution in the vicinity of the corners
  - A priori error estimates
  - A posteriori error estimates
- FEM solution of incompressible flows in tubes with abrupt changes of diameter:
  - Adaptive mesh refinement using a posteriori error estimates
  - A priori error estimates applied to adjusted mesh generation
  - Solution of flows of incompressible viscous fluid with high precision
- Stabilization techniques for FEM
  - Stabilization techniques for FEM using Galerkin Least Squares method
  - Verification by means of a posteriori error estimates
- Numerical experiments

Artificial vascular grafts:

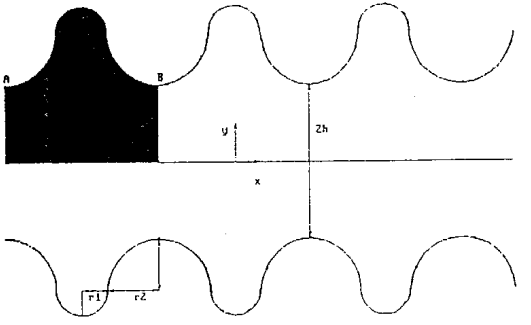

Fig.1 Geometry of the periodic grooved channel with circular corrugations.

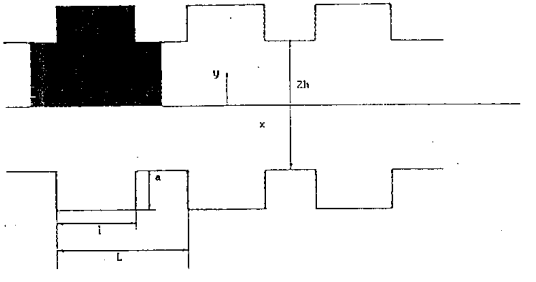

Fig.2 Geometry of the periodic grooved channel with rectangular corrugations.

Fig. 0.1: Profiles of artificial vascular grafts

MAC method results:

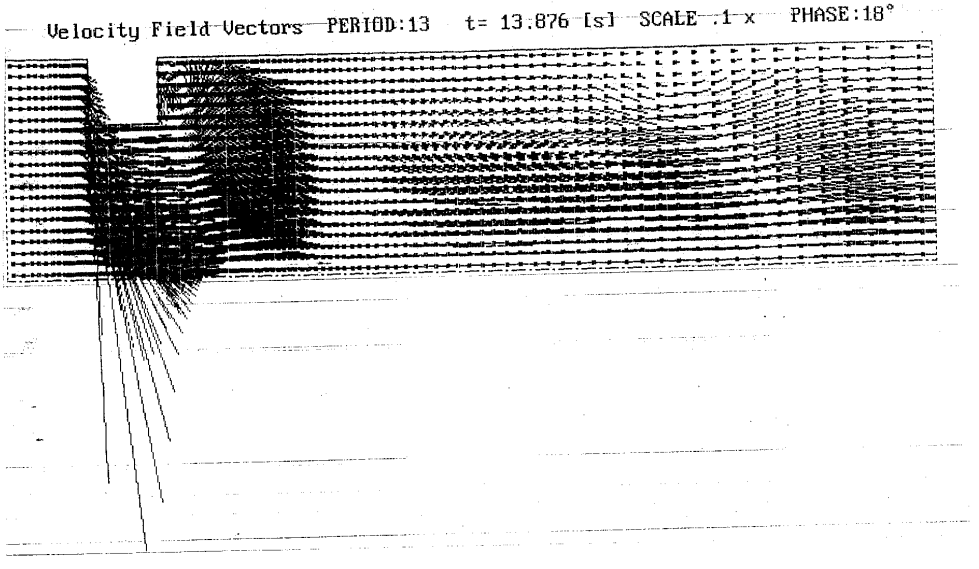

Fig. 0.2: Velocity vectors - pulsatile flow

Contents

1 References 6

2 Navier-Stokes equations for incompressible viscous fluids - classical formulation 7
- 2.1 Unsteady two-dimensional flow . . . 7
- 2.2 Steady two-dimensional flow . . . 8
- 2.3 Steady 2D Stokes problem . . . 8
- 2.4 Unsteady axisymmetric flow . . . 9
- 2.5 Navier-Stokes equations - variational formulation . . . 10

3 Approximation of the problem by FEM 11
- 3.1 Discretization of steady Navier-Stokes equations by FEM . . . 13
- 3.2 Discretization of unsteady Navier-Stokes equations . . . 14
- 3.3 Space semidiscretization of unsteady Navier-Stokes equations by FEM . . . 15
- 3.4 Time discretization of unsteady Navier-Stokes eqs. by the Euler method . . . 16

4 Splitting technique for the Navier-Stokes equations 17

5 Asymptotic behaviour of the solution near corners 18

6 A posteriori error estimates for the Stokes and NS equations 25
- 6.1 The Stokes problem and finite element solution . . . 26
- 6.2 A posteriori error estimate for the Stokes problem . . . 27
- 6.3 A posteriori estimates for 2D steady Navier-Stokes equations . . . 29
- 6.4 Example: determination of the constant C . . . 31

6.5 Application to the adaptive mesh refinement and numerical results 32

7 Application of a priori error estimates for Navier-Stokes equations to very precise solution 36

7.1 Algorithm for generation of computational mesh 37

7.2 Numerical results 42

8 Numerical solution of flow problems by stabilized FEM 47

8.1 Galerkin Least Squares stabilization technique 48

8.2 Results of numerical experiments 50

8.3 Application of a posteriori error estimates 60

9 Conclusion 63

10 References 64

1. References

[1] Girault, V., Raviart, P., G. *Finite Element Method for Navier-Stokes Equations*, Springer, Berlin, 1986

[2] Pironneau, O., Finite Element Methods for Fluids, J. Wiley, Chichester, 1989

[3] Turek, S., Efficient Solvers for Incompressible Flow Problems, Springer, Berlin, 1991

[4] Gresho, P., M., Sani, R., L., Incompressible Flow and the Finite Element Method, J. Wiley, Chichester, 1998

[5] Glowinski, R. *Finite Element Methods for Incompressible Viscous Flow*, Handbook of Numerical Analysis, Vol. IX, Elsevier, 2003

[6] Donea, J., Huerta, A., Finite Element Methods for Flow Problems, J. Wiley, Chichester, 2003

2. Navier-Stokes equations for incompressible viscous fluids - classical formulation

2.1. Unsteady two-dimensional flow

$\Omega \subset \mathbb{R}^2$ ... domain with boundary Γ filled with a fluid
Find $\mathbf{u}(\mathbf{x},t) = (u_1(\mathbf{x},t), u_2(\mathbf{x},t)) \in [\mathcal{C}^2(\Omega)]^2$ *and* $p(\mathbf{x},t) \in \mathcal{C}^1(\Omega)/\mathbb{R}$ *satisfying*

$$\frac{\partial \mathbf{u}}{\partial t} + (\mathbf{u}\cdot\nabla)\mathbf{u} - \nu\Delta\mathbf{u} + \nabla p = \mathbf{f} \quad \text{in } \Omega\times[0,T] \tag{2.1}$$

$$\nabla\cdot\mathbf{u} = 0 \quad \text{in } \Omega\times[0,T] \tag{2.2}$$

Boundary conditions
$$\begin{cases} \mathbf{u} = \mathbf{g} & \text{on } \Gamma_g\times[0,T] \quad \text{(inflow and wall)} \\ -\nu(\nabla\mathbf{u})\mathbf{n} + p\mathbf{n} = \mathbf{0} & \text{on } \Gamma_h\times[0,T] \quad \text{(outflow)} \end{cases}$$

Initial condition $\mathbf{u} = \mathbf{u}_0$ in Ω, $t = 0$

- $\mathbf{u}(\mathbf{x},t)$ ... vector of flow velocity $[m/s]$
- $p(\mathbf{x},t)$ ... pressure divided by density $[Pa\cdot m^3/kg]$
- ν ... kinematic viscosity of the fluid $[m^2/s]$
- $\mathbf{f}(\mathbf{x},t)$ ... vector of intensity of volume forces per mass unit $[N/kg]$
- Γ_g and Γ_h ... subsets of Γ satisfying $\overline{\Gamma} = \overline{\Gamma}_g \cup \overline{\Gamma}_h$
- $\mathbf{n}$ ... unit outer normal vector to the boundary Γ

2.2. Steady two-dimensional flow

For the case of steady flow, the Navier-Stokes equations are reduced to

$$(\mathbf{u}\cdot\nabla)\mathbf{u} - \nu\Delta\mathbf{u} + \nabla p = \mathbf{f} \quad \text{in } \Omega \tag{2.3}$$

$$\nabla\cdot\mathbf{u} = 0 \quad \text{in } \Omega \tag{2.4}$$

and boundary conditions to

$$\mathbf{u} = \mathbf{g} \quad \text{on } \Gamma_g \tag{2.5}$$

$$-\nu(\nabla\mathbf{u})\mathbf{n} + p\mathbf{n} = \mathbf{0} \quad \text{on } \Gamma_h \tag{2.6}$$

2.3. Steady 2D Stokes problem

In case of the Stokes flow the first (nonlinear) term in (2.3) is omitted:

$$-\nu\Delta\mathbf{u} + \nabla p = \mathbf{f} \quad \text{in } \Omega \tag{2.7}$$

$$\nabla\cdot\mathbf{u} = 0 \quad \text{in } \Omega \tag{2.8}$$

and boundary conditions are the same as in (2.5), (2.6).

2.4. Unsteady axisymmetric flow

Now consider the system of Navier-Stokes equations for incompressible viscous fluid in 3D, cf. [19]. Transforming the cartesian system of coordinates $\{x_1, x_2, x_3\}$ into the cylindrical system of coordinates $\{r, \varphi, z\}$ where $x_1 = r\cos\varphi;\ x_2 = r\sin\varphi;\ x_3 = z$, and considering axialy symmetric flow (variables are independent of φ), we obtain Navier-Stokes equations in the form (cf. e.g. [8])

$$\frac{\partial u}{\partial t} + v\frac{\partial u}{\partial r} + u\frac{\partial u}{\partial z} - \nu\left(\frac{\partial^2 u}{\partial r^2} + \frac{1}{r}\frac{\partial u}{\partial r} + \frac{\partial^2 u}{\partial z^2}\right) + \frac{\partial p}{\partial z} = f_z \quad \text{in } \Omega \times [0,T] \tag{2.9}$$

$$\frac{\partial v}{\partial t} + v\frac{\partial v}{\partial r} + u\frac{\partial v}{\partial z} - \nu\left(\frac{\partial^2 v}{\partial r^2} + \frac{1}{r}\frac{\partial v}{\partial r} - \frac{v}{r^2} + \frac{\partial^2 v}{\partial z^2}\right) + \frac{\partial p}{\partial r} = f_r \quad \text{in } \Omega \times [0,T] \tag{2.10}$$

where

$$\frac{\partial v}{\partial r} + \frac{v}{r} + \frac{\partial u}{\partial z} = 0 \quad \text{in } \Omega \times [0,T] \tag{2.11}$$

- u denotes the axial component of velocity (direction of z-coordinate) considered in m/s, which is a function of z, r and t
- v denotes the radial component of velocity (direction of r-coordinate) considered in m/s, which is a function of z, r and t
- $\mathbf{f} = (f_z, f_r)^T$ denotes the density of volume forces per mass unit considered in N/m^3, which could be a function of z, r and t

Equations (2.9)-(2.11) govern the axisymmetric flow in a domain $\Omega \subset \mathbb{R}^2$, where the generic point of $\mathbb{R}^2$ is now denoted by $\mathbf{x} = (z, r)^T$ for arbitrary φ.

2.5. Navier-Stokes equations - variational formulation

Vector function spaces

$$V_g = \left\{ \mathbf{v} = (v_1, v_2) \mid \mathbf{v} \in [H^1(\Omega)]^2; \textbf{Tr } v_i = g_i, i = 1, 2, \text{ on } \Gamma_g \right\}$$
$$V = \left\{ \mathbf{v} = (v_1, v_2) \mid \mathbf{v} \in [H^1(\Omega)]^2; \textbf{Tr } v_i = 0, i = 1, 2, \text{ on } \Gamma_g \right\}$$

Find $\mathbf{u}(\mathbf{x}, t) = (u_1(\mathbf{x}, t), u_2(\mathbf{x}, t)) \in V_g$, $\mathbf{u} - \mathbf{u}_g \in V$ *and* $p(\mathbf{x}, t) \in L_2(\Omega)/\mathbb{R}$ *satisfying for any* $t \in [0, T]$

$$\int_\Omega \frac{\partial \mathbf{u}}{\partial t} \cdot \mathbf{v} \mathrm{d}\Omega + \int_\Omega (\mathbf{u} \cdot \nabla)\mathbf{u} \cdot \mathbf{v} \mathrm{d}\Omega + \nu \int_\Omega \nabla \mathbf{u} : \nabla \mathbf{v} \mathrm{d}\Omega - \int_\Omega p \nabla \cdot \mathbf{v} \mathrm{d}\Omega = \int_\Omega \mathbf{f} \cdot \mathbf{v} \mathrm{d}\Omega$$
$$\int_\Omega \psi \nabla \cdot \mathbf{u} \mathrm{d}\Omega = 0$$

for $\mathbf{v} \in V$ *and* $\psi \in L_2(\Omega)$.

- $\mathbf{u}_g \in V_g$ is a representation of the Dirichlet boundary condition $\mathbf{g}$
- $\nabla \mathbf{u} : \nabla \mathbf{v} = \frac{\partial u_x}{\partial x}\frac{\partial v_x}{\partial x} + \frac{\partial u_x}{\partial y}\frac{\partial v_x}{\partial y} + \frac{\partial u_y}{\partial x}\frac{\partial v_y}{\partial x} + \frac{\partial u_y}{\partial y}\frac{\partial v_y}{\partial y}$

3. Approximation of the problem by FEM

- Divide Ω into N finite elements T_K such that

$$\bigcup_{K=1}^{N} \overline{T}_K = \overline{\Omega},\ \mu_{\mathbb{R}^2}\left(T_K \cap T_L\right) = 0, K \neq L$$

- Taylor-Hood finite elements(cf. Fig. 3.1) – function spaces for approximation:

velocities

$$V_{gh} = \left\{ \mathbf{v}_h = (v_{h_1}, v_{h_2}) \in [\mathcal{C}(\overline{\Omega})]^2;\ v_{h_i}\,|_{T_K} \in R_2(\overline{T_K}),\ i = 1,2,\ \mathbf{v}_h = \mathbf{g} \text{ in nodes on } \Gamma_g \right\}$$

pressure and test functions for the continuity equation

$$Q_h = \left\{ \psi_h \in \mathcal{C}(\overline{\Omega});\ \psi_h\,|_{T_K} \in R_1(\overline{T_K}) \right\}$$

test functions for momentum equations

$$V_h = \left\{ \mathbf{v}_h = (v_{h_1}, v_{h_2}) \in [\mathcal{C}(\overline{\Omega})]^2;\ v_{h_i}\,|_{T_K} \in R_2(\overline{T_K}),\ i = 1,2,\ \mathbf{v}_h = \mathbf{0} \text{ in nodes on } \Gamma_g \right\}$$

where

$$R_m(\overline{T_K}) = \begin{cases} P_m(\overline{T_K}), & \text{if } T_K \text{ is a triangle} \\ Q_m(\overline{T_K}), & \text{if } T_K \text{ is a quadrilateral} \end{cases}$$

Taylor-Hood elements:

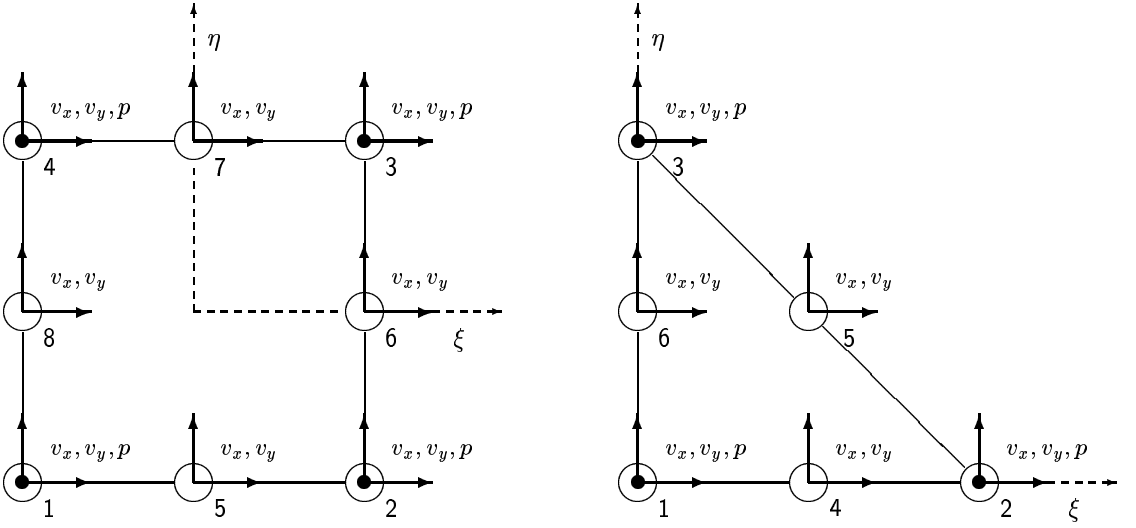

Fig. 3.1: Taylor-Hood elements: quadrilateral - left, tringle - right

Taylor-Hood elements satisfy Babuška-Brezzi condition (inf-sup condition)

$$\exists_{C_B>0,const.}\ \forall_{q_h\in Q_h}\ \exists_{\mathbf{v}_h\in V_{gh}}\ (q_h, \nabla\cdot\mathbf{v}_h)_0 \geq C_B\|q_h\|_0\|\mathbf{v}_h\|_1. \tag{3.1}$$

3.1. Discretization of steady Navier-Stokes equations by FEM

Consider the variational formulation of the steady Navier-Stokes equations. Since the function spaces satisfy $V_{gh} \subset V_g$, $V_h \subset V$, and $Q_h \subset L_2(\Omega)/\mathbb{R}$ for prescribed arbitrary value of pressure (e.g. $p_h = 0$) in one node, we can introduce *approximate steady Navier-Stokes problem*:

Seek $\mathbf{u}_h \in V_{gh}$ and $p_h \in Q_h$ satisfying

$$\int_\Omega (\mathbf{u}_h \cdot \nabla)\mathbf{u}_h \cdot \mathbf{v}_h \mathrm{d}\Omega$$

$$+\nu \int_\Omega \nabla \mathbf{u}_h : \nabla \mathbf{v}_h \mathrm{d}\Omega - \int_\Omega p_h \nabla \cdot \mathbf{v}_h \mathrm{d}\Omega = \int_\Omega \mathbf{f} \cdot \mathbf{v}_h \mathrm{d}\Omega, \ \forall \mathbf{v}_h \in V_h \tag{3.2}$$

$$\int_\Omega \psi_h \nabla \cdot \mathbf{u}_h \mathrm{d}\Omega = 0, \ \forall \psi_h \in Q_h \tag{3.3}$$

$$\mathbf{u}_h - \mathbf{u}_{gh} \in V_h \tag{3.4}$$

where $\mathbf{u}_{gh} \in V_{gh}$ is the projection of $\mathbf{u}_g$ onto the space V_{gh}.

Using the shape regular triangulation and refining the mesh such that $h_{max} \to 0$ where

$$h_{max} = \max_K h_K,$$

the solution of the approximated problem converges to the solution of the continuous problem (for more cf. e.g. Brezzi, Fortin [4]).

3.2. Discretization of unsteady Navier-Stokes equations

To solve the unsteady Navier-Stokes equations (2.1)-(2.2), we need to discretize the system both in space and time. Two techniques are avaiable:

- Method of lines (MOL)
  1. step – semidiscretization in space (e.g. by FEM)
  2. step – discretization in time (e.g. by the Euler method)
- Rothe's method
  1. step – semidiscretization in time
  2. step – discretization in space

3.3. Space semidiscretization of unsteady Navier-Stokes equations by FEM

Let us perform space semidiscretization of the system (2.1)-(2.2) by the FEM in the context of the MOL. Extending derivations for the steady case in Chapter 3.1, we introduce the problem:

Seek $\mathbf{u}_h(t) \in V_{gh},\ t \in [0,T]$ and $p_h(t) \in Q_h,\ t \in [0,T]$ satisfying

$$\begin{aligned}
\int_\Omega \frac{\partial \mathbf{u}_h}{\partial t} \cdot \mathbf{v}_h \mathrm{d}\Omega + \int_\Omega (\mathbf{u}_h \cdot \nabla)\mathbf{u}_h \cdot \mathbf{v}_h \mathrm{d}\Omega \ &+\ \nu \int_\Omega \nabla \mathbf{u}_h : \nabla \mathbf{v}_h \mathrm{d}\Omega - \\
- \int_\Omega p_h \nabla \cdot \mathbf{v}_h \mathrm{d}\Omega \ &=\ \int_\Omega \mathbf{f} \cdot \mathbf{v}_h \mathrm{d}\Omega,\ \forall \mathbf{v}_h \in V_h \qquad (3.5)\\
\int_\Omega \psi_h \nabla \cdot \mathbf{u}_h \mathrm{d}\Omega \ &=\ 0,\ \forall \psi_h \in Q_h \qquad (3.6)\\
\mathbf{u}_h - \mathbf{u}_{gh} \ &\in\ V_h \qquad (3.7)
\end{aligned}$$

3.4. Time discretization of unsteady Navier-Stokes eqs. by the Euler method

Consider partition of the time interval $[0, T]$ into M time intervals with $M + 1$ time layers. The constant time step between n-th and $(n + 1)$-st time layer is denoted by ϑ.

Apply the implicit Euler method (backward difference method), i.e. time derivative is substituted as

$$\frac{\partial \mathbf{u}_h}{\partial t} \approx \frac{\mathbf{u}_h^{n+1} - \mathbf{u}_h^n}{\vartheta}.$$

This leads to fully implicit method for seeking $\mathbf{u}_h$ in $(n + 1)$-st time layer:

Seek $\mathbf{u}_h^{n+1} \in V_{gh}$ and $p_h^{n+1} \in Q_h$ satisfying

$$\begin{aligned}
\frac{1}{\vartheta}\int_\Omega \mathbf{u}_h^{n+1}\cdot\mathbf{v}_h \mathrm{d}\Omega + \int_\Omega (\mathbf{u}_h^{n+1}\cdot\nabla)\mathbf{u}_h^{n+1}\cdot\mathbf{v}_h \mathrm{d}\Omega \;&+\; \nu\int_\Omega \nabla\mathbf{u}_h^{n+1} : \nabla\mathbf{v}_h \mathrm{d}\Omega - \\
-\int_\Omega p_h^{n+1}\nabla\cdot\mathbf{v}_h \mathrm{d}\Omega - \frac{1}{\vartheta}\int_\Omega \mathbf{u}_h^n\cdot\mathbf{v}_h \mathrm{d}\Omega \;&=\; \int_\Omega \mathbf{f}^{n+1}\cdot\mathbf{v}_h \mathrm{d}\Omega,\ \forall\mathbf{v}_h \in V_h \qquad (3.8)\\
\int_\Omega \psi_h \nabla\cdot\mathbf{u}_h^{n+1}\mathrm{d}\Omega \;&=\; 0,\ \forall\psi_h \in Q_h \qquad (3.9)\\
\mathbf{u}_h^{n+1} - \mathbf{u}_{gh}^{n+1} \;&\in\; V_h \qquad (3.10)
\end{aligned}$$

Resulting nonlinear algebraic system is then solved by the Newton method.

4. Splitting technique for the Navier-Stokes equations

Apply the idea of splitting to the Navier-Stokes equations (2.1), (2.2) e.g. as done by R. Glowinski in [19]:

Initially put: $\mathbf{u}^0 = \mathbf{u}_0$.

Then for $n \geq 0$, we obtain $\mathbf{u}^{n+1}$ from $\mathbf{u}^n$ via

$$\text{Stokes} \begin{cases} \frac{\partial \mathbf{u}}{\partial t} - \nu \Delta \mathbf{u} + \nabla p = \mathbf{f} \quad \text{in } \Omega \times [t^n, t^{n+1}], \\ \nabla \cdot \mathbf{u} = 0 \quad \text{in } \Omega \times [t^n, t^{n+1}], \\ \mathbf{u}(t^n) = \mathbf{u}^n, \\ \mathbf{u} = \mathbf{g} \ \text{ on } \ \partial\Omega \times [t^n, t^{n+1}], \end{cases} \tag{4.1}$$

$$\mathbf{u}^{n+\frac{1}{2}} = \mathbf{u}(t^{n+1}), \tag{4.2}$$

$$\text{transport} \begin{cases} \frac{\partial \mathbf{u}}{\partial t} + (\mathbf{u}^{n+\frac{1}{2}} \cdot \nabla)\mathbf{u} = 0 \quad \text{in } \Omega \times [0, \Delta t], \\ \mathbf{u}(0) = \mathbf{u}^{n+\frac{1}{2}}, \\ \mathbf{u} = \mathbf{g}^{n+1} (= \mathbf{u}^{n+\frac{1}{2}}) \ \text{ on } \ \Gamma_-^{n+1} \times [0, \Delta t], \end{cases} \tag{4.3}$$

$$\mathbf{u}^{n+1} = \mathbf{u}(\Delta t), \tag{4.4}$$

Here
$$\Gamma_-^{n+1} = \{x |\ x \in \partial\Omega,\ \mathbf{g}^{n+1}(x) \cdot \mathbf{n}(x) < 0\}, \tag{4.5}$$

means the inflou part of the boundary ($\mathbf{n}(x)$ is the outgoing normal).

5. Asymptotic behaviour of the solution near corners

Introduction

- Motivation: numerical solution of flow of incompressible fluid in tubes with abrupt changes of diameter.
- We study the axisymmetric flow governed by the Navier-Stokes equations.
- Concern in the asymptotic behaviour of the solution near the corners.
- The asymptotic behaviour of the exact solution of the NSE in the vicinity of the corner is obtained using some symmetry of the principal part of the Stokes equation, and then applying the Fourier transform.
- Our aim is to make use of the information on the local behaviour of the solution near the corner point, in order to suggest local meshing subordinate to the asymptotics.
- Later we present a cheap strategy to be applied to families of triangular elements.

Solution of Navier-Stokes equations near the corner - the axisymmetric case

- The asymptotics of the biharmonic equation for the stream function ψ are basic.
- Here we concentrate on *pipe flow* (axially symmetric).

The stream function - vorticity formulation in cylindrical geometry:

$$\frac{\partial \omega}{\partial t} + u_1 \frac{\partial \omega}{\partial z} + u_2 \frac{\partial \omega}{\partial r} + u_2 \frac{\omega}{r} = \nu \left(\frac{\partial^2 \omega}{\partial z^2} + \frac{\partial^2 \omega}{\partial r^2} + \frac{1}{r}\frac{\partial \omega}{\partial r} - \frac{\omega}{r^2} \right), \qquad (5.1)$$

$$\frac{\partial^2 \psi}{\partial z^2} + \frac{\partial^2 \psi}{\partial r^2} - \frac{1}{r}\frac{\partial \psi}{\partial r} = -r\omega\,, \qquad (5.2)$$

$$u_1 = \frac{1}{r}\frac{\partial \psi}{\partial r}\,, \qquad (5.3)$$

$$u_2 = -\frac{1}{r}\frac{\partial \psi}{\partial z}\,, \qquad (5.4)$$

- ω is the vorticity,
- ψ is the stream function,
- r, z are cylindrical coordinates,
- $u_1 = V_z, u_2 = V_r$ are in turn axial and radial velocity components,
- ν is the viscosity.

The Stationary Flow

Substituting ω, u_1, u_2 from (5.2) – (5.4) into (5.1), and substituting

$$z - z_0 = x, \quad r - r_0 = y,$$

we get, on a model domain Ω_0 (see Fig. 5), with the internal angle ω, $0 < \omega \leq 2\pi$:

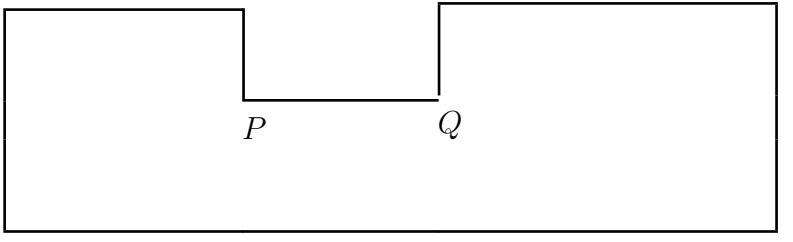

Fig. 5.1: The solution domain Ω

$$
\begin{aligned}
&- \frac{1}{(y+r_0)^2}\frac{\partial\psi}{\partial y}\frac{\partial^3\psi}{\partial x^3} - \frac{1}{(y+r_0)^2}\frac{\partial\psi}{\partial y}\frac{\partial^3\psi}{\partial x\partial y^2} + \frac{1}{(y+r_0)^3}\frac{\partial\psi}{\partial y}\frac{\partial^2\psi}{\partial x\partial y} + \\
&+ \frac{1}{(y+r_0)^2}\frac{\partial\psi}{\partial x}\frac{\partial^3\psi}{\partial x^2\partial y} + \frac{1}{(y+r_0)^2}\frac{\partial\psi}{\partial x}\frac{\partial^3\psi}{\partial y^3} - \frac{1}{(y+r_0)^4}\frac{\partial\psi}{\partial x}\frac{\partial\psi}{\partial y} = \\
&= \nu\,\{\frac{1}{y+r_0}(\frac{\partial^4\psi}{\partial y^4} + 2\frac{\partial^4\psi}{\partial y^2\partial x^2} + \frac{\partial^4\psi}{\partial x^4}) - \qquad (5.5)\\
&- \frac{1}{(y+r_0)^2}(\frac{\partial^3\psi}{\partial x^3} + \frac{\partial^3\psi}{\partial x^2\partial y} + \frac{\partial^3\psi}{\partial x\partial y^2} + \frac{\partial^3\psi}{\partial y^3}) + \frac{3}{(y+r_0)^3}\frac{\partial^2\psi}{\partial x^2} - \frac{3}{(y+r_0)^4}\frac{\partial\psi}{\partial x}\},
\end{aligned}
$$

We first restrict ourselves to the principal part part of equation (5.5), namely

$$\frac{\partial^4\psi}{\partial x^4} + 2\frac{\partial^4\psi}{\partial x^2\partial y^2} + \frac{\partial^4\psi}{\partial y^4} \;=\; f, \tag{5.6}$$

where we first assume $f = 0$.

The boundary conditions are

$$\psi\Big|_{\partial\Omega_0} = 0, \quad \frac{\partial\psi}{\partial n}\Big|_{\partial\Omega_0} = 0$$

where n is the outgoing normal to the boundary $\partial\Omega_0$.

Using polar coordinates $\rho,\ \vartheta$,

$$x \;= \rho\ \cos\vartheta, \quad y \;= \rho\ \sin\vartheta,$$

on the infinite cone $\widetilde{\Omega}_0$:

$$\widetilde{\Omega}_0 = \{(\rho,\vartheta),\ 0 < \rho < \infty,\ \alpha < \vartheta < \beta\}, \tag{5.7}$$

where $\beta - \alpha = \omega$, and substituting

$$\tau = \ln\frac{1}{\rho}, \tag{5.8}$$

we get

$$[(\psi_{\tau\tau\tau\tau} + 4\psi_{\tau\tau\tau} + 4\psi_{\tau\tau}) + 4\psi_{\tau\vartheta\vartheta} + 2\psi_{\tau\tau\vartheta\vartheta} + \psi_{\vartheta\vartheta\vartheta\vartheta} + 4\psi_{\vartheta\vartheta}] \;=\; 0 \tag{5.9}$$

on the infinite strip

$$\tau \in (-\infty, +\infty)\ ,\ \vartheta \in (\alpha,\beta). \tag{5.10}$$

Performing the Fourier transform with respect to τ,

$$\widehat{\psi}(\lambda,\vartheta) = (2\pi)^{-1/2}\int_{-\infty}^{+\infty} e^{-\mathrm{i}\lambda\tau}\psi(\tau,\vartheta)d\tau, \tag{5.11}$$

Eq. (5.9) transforms to the ordinary differential equation

$$\widehat{L}(\vartheta,\mathrm{i}\lambda)\widehat{\psi} \equiv \widehat{\psi}_{\vartheta\vartheta\vartheta\vartheta} + (-2\lambda^2 + 4\mathrm{i}\lambda + 4)\widehat{\psi}_{\vartheta\vartheta} + (\lambda^4 - 4\mathrm{i}\lambda^3 - 4\lambda^2)\widehat{\psi} \;=\; 0, \tag{5.12}$$

where $\vartheta \in (\alpha,\beta)$. The operator $\widehat{L}$ has the inverse operator $R(\lambda)$ which is a meromorphic operator-valued function of λ, each pole of $R(\lambda)$ having finite multiplicity.

Eq. (5.12) is a fourth order equation with constant coefficients, the characteristic equation is the biquadratic equation

$$\mu^4 + (-2\,\lambda^2 + 4\,\mathrm{i}\,\lambda + 4)\mu^2 + (\lambda^4 - 4\,\mathrm{i}\,\lambda^3 - 4\lambda^2) = 0. \tag{5.13}$$

And the solutions of (5.13) are

$$\mu_{1,2} \;=\; \pm\lambda, \qquad \mu_{3,4} \;=\; \pm(\lambda - 2\mathrm{i}). \tag{5.14}$$

Now we are in the position to use the following theorem by Kondratiev, Olejnik [25].

Theorem 5.1 *Let $f \in \mathring{W}^{k_1}_{\delta_1}(\widetilde{\Omega}_0)$ and let $\psi \in \mathring{W}^{k+4}_{\delta}(\widetilde{\Omega}_0)$ be the solution of (5.6) satisfying the boundary conditions (5.7) on $\partial\widetilde{\Omega}$. Let*

$$h_1 \equiv \frac{-\delta_1 + 2k_1 + 6}{2} > \frac{-\delta + 2k + 6}{2} \equiv h \ , \ k_1 \geq k. \tag{5.15}$$

Suppose that the resolvent function $R(\lambda)$ has no poles on the line Im $\lambda = h_1$.

Then the solution ψ has the form

$$\psi(x,y) = \sum_j \sum_{s=0}^{p_j - 1} a_{js} \rho^{-i\lambda_j} \ln^s \rho \cdot \psi_{sj}(\vartheta) \ + \ w(x,y), \tag{5.16}$$

where w satisfies (5.7), $w \in \mathring{W}^{k_1+4}_{\delta_1}(\widetilde{\Omega}_0)$, $\psi_{sj} \in C^\infty(\widetilde{\Omega}_0)$, $a_{js} = const.$, and λ_j are the poles of multiplicity p_j of the function $R(\lambda)$, satisfying

$$h < \mathrm{Im}\lambda_j < h_1.$$

Now we can apply Theorem 5.1 to Eq. (5.6), with $k = 0, \ \delta = 4$. We put $h_1 = 2$, $k_1 = 0, \ \delta_1 = 2$.

Theorem 5.1 deals with the infinite cone $\widetilde{\Omega}_0$. The situation is a bit more complicated in the conical domain Ω_0, and we refer to B. [5].

Finding the poles of $R(\lambda)$: According to (5.14), the general solution of (5.12) is

$$\widehat{\psi} \;=\; c_1 \exp(\lambda\vartheta) + c_2 \exp(-\lambda\vartheta) + c_3 \sin(2\vartheta) + c_4 \cos(2\vartheta). \tag{5.17}$$

The boundary conditions are

$$\widehat{\psi}\Big|_{\vartheta=\alpha,\beta} = 0, \qquad \frac{\partial\widehat{\psi}}{\partial\vartheta}\Big|_{\vartheta=\alpha.\beta} = 0, \tag{5.18}$$

Nontrivial solution of (5.17), (5.18) exists iff

$$R(\lambda) \equiv \det \begin{pmatrix} \exp(\lambda\alpha) & \exp(\lambda\beta) & \lambda\exp(\lambda\alpha) & \lambda\exp(\lambda\beta) \\ \exp(-\lambda\alpha) & \exp(-\lambda\beta) & -\lambda\exp(-\lambda\alpha) & -\lambda\exp(-\lambda\beta) \\ \sin(2\alpha) & \sin(2\beta) & 2\cos(2\alpha) & 2\cos(2\beta) \\ \cos(2\alpha) & \cos(2\beta) & -2\sin(2\alpha) & -2\sin(2\beta) \end{pmatrix} = 0. \tag{5.19}$$

E.g. for $\omega = \frac{3}{2}\pi$ $(\alpha = 0,\ \beta = \frac{3}{2}\pi)$ the first root of (5.19) is $\mathrm{i}\lambda_1 = -1.54448374$, which is simple, and by Theorem 5.1, the first term of the expansion is $\rho^{1.54448374}$, i.e.

$$\psi(\rho,\vartheta) = \rho^{1.54448374}\ \phi(\vartheta) \ +\ \dots\ . \tag{5.20}$$

By (5.3), (5.4), we get for the velocities, the expansion

$$u_l(\rho,\vartheta) = \rho^{0.54448374}\varphi_l(\vartheta) + \dots,\ l = 1,2, \tag{5.21}$$

where the functions φ_l do not depend on ρ.

The same result in desk geometry by Kondratiev [24], Ladevéze, Peyret [26], M. Dauge [15], where $\psi^{desk}(\rho,\vartheta) = \rho^{1.5445}\ \phi^d(\vartheta) \ +\ \dots\ .$

6. A posteriori error estimates for the Stokes and NS equations

Introduction

- At present various a posteriori error estimates for the Stokes problem are available, e.g. M. Ainsworth, J.T. Oden [2], R. Verfürth [28], other references in B. [6].
- Here focus on the constant in the estimate - significant in adaptivity.
- We derive own a posteriori estimate and trace the colorblue constants and their sources.
- In B. [6] and B. [7] a posteriori estimates for the Stokes problem in a 2D and 3D.
- Discussion of adaptive stratey
- Numerical results for a model of flow in a domain with corner singularity.

6.1. The Stokes problem and finite element solution

The Stokes problem in 2D: $\Omega \subset I\!R^2$ bounded Lipschitzian domain, given $\boldsymbol{f} \in L^2(\Omega)$, find $\{\boldsymbol{u}, p\} \in H^1(\Omega)^2 \times L^2_0(\Omega)$ such that, in the weak sense,

$$\begin{aligned} -\nu\Delta\boldsymbol{u} + \nabla p &= \boldsymbol{f} \quad \text{in } \Omega\ , \\ \text{div } \boldsymbol{u} &= 0 \quad \text{in } \Omega\ , \\ \boldsymbol{u} &= \boldsymbol{0} \quad \text{on } \partial\Omega\ , \end{aligned} \tag{6.1}$$

where $\boldsymbol{u}$ is the velocity vector, p is the presure, $\nu > 0$ is the viscosity. $L^2_0(\Omega)$ is the space of L^2 functions having mean value zero. Let us denote $(.,.)_0$ the scalar product in L^2, and denote $X = H^1_0(\Omega)^2 \times L^2_0(\Omega)$.

Stokes problem (6.1) variationally: find $\{\boldsymbol{u}, p\} \in X$

$$\nu(\nabla\boldsymbol{u}, \nabla\boldsymbol{u}_*)_0 - (p, \text{div } \boldsymbol{u}_*)_0 + (p_*, \text{div } \boldsymbol{u})_0 = (\boldsymbol{f}, \boldsymbol{u}_*)_0 \quad \forall\{\boldsymbol{u}_*, p_*\} \in X. \tag{6.2}$$

Finite Element Approximation

For the FEM approximation take Ω a polygon in $I\!R^2$, for simplicity.

Let $\{\mathcal{T}_h\}_{h\to 0}$ be a regular (cf. [18]) family of triangulations of Ω.

V_h, Q_h the finite element spaces of Taylor - Hood elements, velocities and pressure are approximated as continuous functions of spatial variables.

The FEM approximation: find $\{\boldsymbol{u}^h, p^h\} \in V_h \times Q_h$ such that, $\forall\{\boldsymbol{u}^h_*, p^h_*\} \in V_h \times Q_h$,

$$\nu(\nabla\boldsymbol{u}^h, \nabla\boldsymbol{u}^h_*)_0 - (p^h, \text{div } \boldsymbol{u}^h_*)_0 + (p^h_*, \text{div } \boldsymbol{u}^h)_0 = (\boldsymbol{f}, \boldsymbol{u}^h_*)_0\ . \tag{6.3}$$

6.2. A posteriori error estimate for the Stokes problem

Define the residual components on the elements $K \in \mathcal{T}^h$, by:

$$\boldsymbol{R}_1(\boldsymbol{u}^h, p^h) = \boldsymbol{f} + \nu \Delta \boldsymbol{u}^h - \nabla p^h, \quad R_2(\boldsymbol{u}^h, p^h) = \text{div } \boldsymbol{u}^h. \tag{6.4}$$

The error components are defined on Ω by

$$\boldsymbol{e}_u = \boldsymbol{u} - \boldsymbol{u}^h \ , \ e_p = p - p^h \ ,$$

where $\{\boldsymbol{u}, p\}$ is the exact solution defined in (6.2), $\{\boldsymbol{u}^h, p^h\}$ is the approximate solution, by (6.3). The X norm of $\{\boldsymbol{e}_u, e_p\}$ is

$$\|\{\boldsymbol{e}_u, e_p\}\|_X^2 = (\boldsymbol{e}_u, \boldsymbol{e}_u)_1 + (e_p, e_p)_0.$$

Using the Poincaré-Friedrichs inequality, the Galerkin orthogonality, the Schwarz inequality, the interpolation properties of V^h, Q^h, and the estimate of the solution of the dual problem, we get the theorem (proof in B. [6] is based on the ideas of Eriksson et al. [16], and Babuška and Rheinboldt [3])

Theorem 6.2 *Let Ω be a polygon in $\mathbb{R}^2$. with Lipschitz continuous boundary. Let $\mathcal{T}^h$ be a regular family of triangulations of Ω. Let $\{\boldsymbol{u}^h, p^h\}$ be the Hood-Taylor approximation of the solution $\{\boldsymbol{u}, p\}$ of the Stokes problem. Then the error $\{\boldsymbol{e}_u, e_p\}$ satisfies the following a posteriori estimate*

$$\|\boldsymbol{e}_u\|_1 + \|e_p\|_0 \;\leq\; 2\, C_P\, C_I\, C_R \sum_{K\in\mathcal{T}^h} \left(h_K \|\boldsymbol{R}_1(\boldsymbol{u}^h, p^h)\|_{0,K} + \right. \tag{6.5}$$

$$\left. + \|R_2(\boldsymbol{u}^h, p^h)\|_{0,K} + h_K^{\frac{1}{2}} \sum_{l\in\partial K} \left\| \frac{1}{2} \left[\!\left[\nu \frac{\partial \boldsymbol{u}^h}{\partial \boldsymbol{n}} \right]\!\right]_l \right\|_{0,l} \right),$$

where C_P, C_I, C_R are positive constants.

Remarks The constants $C_P, C_I,$ and C_R in Theorem 6.2 come in turn from the Poincaré inequality, the interpolation properties of V_h, Q_h, and the regularity of the dual problem, respectively.

Our result in Theorem 6.2 is in agreement with that of R. Verfürth [28], though the technique of the proof is different, and we do not require any regularity.

6.3. A posteriori estimates for 2D steady Navier-Stokes equations

Consider steady Navier-Stokes problem (2.1), (2.2), with boundary conditions (2.3). Discretization by finite elements again with Taylor - Hood elements P2/P1.
Exact solution denoted by (u_1, u_2, p) and the approximate FEM solution by (u_1^h, u_2^h, p_h).
The difference is the error

$$(e_{u_1}, e_{u_2}, e_p) \equiv (u_1 - u_1^h, u_2 - u_2^h, p - p_h). \tag{6.6}$$

For the solution (u_1, u_2, p) we denote

$$\mathcal{U}^2(u_1, u_2, p, \Omega) \equiv \|(u_1, u_2, p)\|_V^2 \equiv \|(u_1, u_2)\|_{1,\Omega}^2 + \|p\|_{0,\Omega}^2 \tag{6.7}$$
$$\equiv \int_\Omega \left(u_1^2 + u_2^2 + \left(\frac{\partial u_1}{\partial x}\right)^2 + \left(\frac{\partial u_1}{\partial y}\right)^2 + \left(\frac{\partial u_2}{\partial x}\right)^2 + \left(\frac{\partial u_2}{\partial y}\right)^2 \right) \mathrm{d}\Omega + \int_\Omega p^2 \mathrm{d}\Omega.$$

The estimate in Theorem 6.2 can be generalized to the Navier-Stokes equations:

$$\|(e_{u_1}, e_{u_2})\|_{1,\Omega}^2 + \|e_p\|_{0,\Omega}^2 \leq \mathcal{E}^2(u_1^h, u_2^h, p^h), \tag{6.8}$$

where (cf. [28])

$$\mathcal{E}^2(u_1^h, u_2^h, p^h, \Omega) \equiv C \left[\sum_{K \in \mathcal{T}^h} h_K^2 \int_{T_K} (r_1^2 + r_2^2) + \sum_{K \in \mathcal{T}^h} \int_{T_K} r_3^2 \mathrm{d}\Omega \right], \tag{6.9}$$

where h_K denotes the diameter of the element T_K and $r_i,\ i = 1, 2, 3$, are the residuals

$$r_1 = f_x - \left(u_1^h \frac{\partial u_1^h}{\partial x} + u_2 \frac{\partial u_1^h}{\partial y} \right) + \nu \left(\frac{\partial^2 u_1^h}{\partial x^2} + \frac{\partial^2 u_1^h}{\partial y^2} \right) - \frac{\partial p^h}{\partial x}, \tag{6.10}$$

$$r_2 = f_y - \left(u_1^h \frac{\partial u_2^h}{\partial x} + u_2^h \frac{\partial u_2^h}{\partial y} \right) + \nu \left(\frac{\partial^2 u_2^h}{\partial x^2} + \frac{\partial^2 u_2^h}{\partial y^2} \right) - \frac{\partial p^h}{\partial y}, \tag{6.11}$$

$$r_3 = \frac{\partial u_1^h}{\partial x} + \frac{\partial u_2^h}{\partial y}. \tag{6.12}$$

Let us note that due to our practical experience we use only the element residuals. Denote also

$$\mathcal{E}^2(u_1^h, u_2^h, p^h, T_K) \equiv C \left[h_K^2 \int_{T_K} (r_1^2 + r_2^2) + \int_{T_K} r_3^2 \mathrm{d}\Omega \right]. \tag{6.13}$$

Qualitatively the value of the constant C not simple to determine, the sources seen in Theorem 6.2. Important: C doesn't depent on the mesh size and so can be determined experimentally for general situation.

By computing of the estimates (6.8) we obtain absolute numbers, that will depend on given quantities in different problems. We are mainly interested in the error related to the computed solution, i.e. relative error. This is given by the ratio of absolute norm of the solution error, related to unit area of the element T_K, $\frac{1}{|T_K|}\ \mathcal{E}^2(u_1^h, u_2^h, p^h, T_K)$, and the solution norm on the whole domain Ω, related to unit area $\frac{1}{|\Omega|}\ \|(u_1^h, u_2^h, p^h)\|^2_{V,\Omega}$, i.e.

$$\mathcal{R}^2(u_1^h, u_2^h, p^h, T_K) = \frac{|\Omega|\ \mathcal{E}^2(u_1^h, u_2^h, p^h, T_K)}{|T_K|\ \|(u_1^h, u_2^h, p^h)\|^2_{V,\Omega}}. \tag{6.14}$$

6.4. Example: determination of the constant C

Example. Steady Stokes equations on one element, $\Omega = [0;2] \times [0;2]$. Let the exact solution and corresponding boundary conditions be given as follows

$$\begin{aligned} v_1 &= 1 + x^3, \\ v_2 &= -3x^2 y, \\ p &= 3\nu x^2 - 3\nu y^2, \quad x \in [0;2], \quad y \in [0;2], \end{aligned}$$

and FEM solution

$$\begin{aligned} v_1^h &= 3x^2 - 2x + 1, \\ v_2^h &= -3x^2 y, \\ p^h &= -0.04xy + bx + cy, \text{ where } b = 0.1133333, \ c = -0.0333333. \end{aligned}$$

To determine the constant C in the estimate (6.8)we compute

$$\begin{aligned} \mathcal{E}^2(v_1^h, v_2^h, p^h) &= C \left\{ h^2 \int_\Omega \left[(ay + b - 6\nu)^2 + (ax + c + 6\nu y)^2 \right] \mathrm{d}x\mathrm{d}y \right. \\ &+ \left. \int_\Omega (3x^2 - 6x + 2)^2 \mathrm{d}x\mathrm{d}y \right\} = \boxed{C \cdot \ 3.2838824}. \end{aligned}$$

Then calculate

$$\|(v_1 - v_1^h, v_2 - v_2^h, p - p^h)\|_{analytical} = \boxed{3.5129774}.$$

And so we get

$$\boxed{C = 1.069754}.$$

6.5. Application to the adaptive mesh refinement and numerical results

Consider 2D flow of viscous, incompressible fluid in the domain with corner singularity (see. Fig. 6.1).

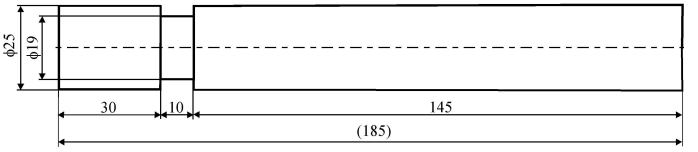

Fig. 6.1: Geometry of the channel

Due to symmetry, we solve the problem only on half of the channel, cf. Fig. 6.2. BC: on the inflow: parabolic velocity profile, at the outflow: 'do nothing' BC. On the upper wall: no-slip condition and on the lower wall: condition of symmetry (i.e. only $y-$component of velocity equals zero). The parameters: $\nu = 0.0001$ m^2/s, $v_{in} = 1$ m/s. The initial mesh is in Fig. 6.2. Relative errors on the elements of the initial mesh are on Fig. 6.3.

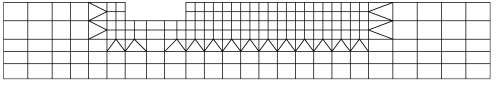

Fig. 6.2: Initial finite element mesh

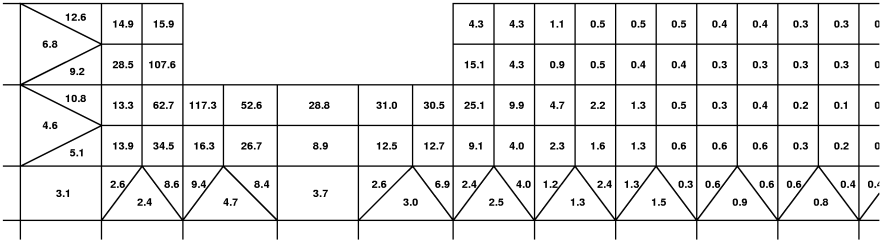

Fig. 6.3: Relative errors on elements of initial mesh

Elements, where the relative error exceeds 3 % are refined, and new solution together with new error estimates is computed. The refinements are on Figures 6.4 to 6.6. The relative errors near the corners are shown on Figures 6.3, 6.8. Numerical results of velocity components, for pressure and streamlines are on Fig. 6.7. The corner singularities caused by nonconvex corners seem to be approximated with high accuracy.

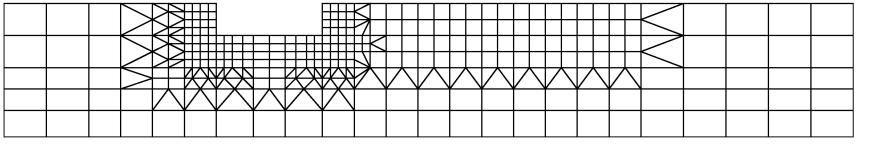

Fig. 6.4: Finite element mesh after first refinement

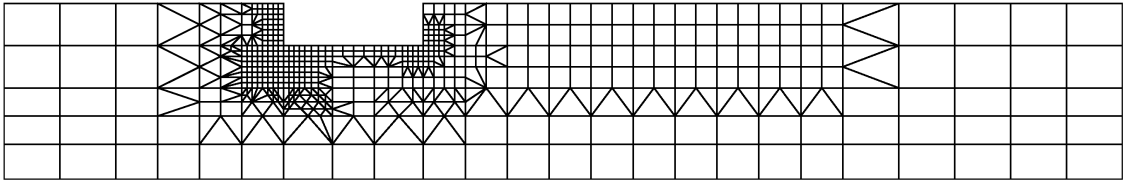

Fig. 6.5: Finite element mesh after second refinement

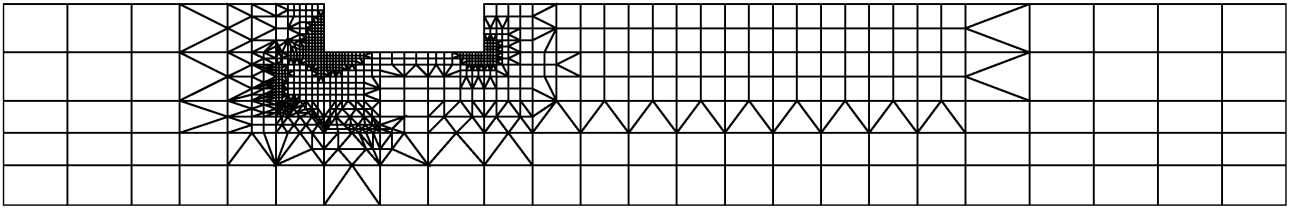

Fig. 6.6: Finite element mesh after third refinement

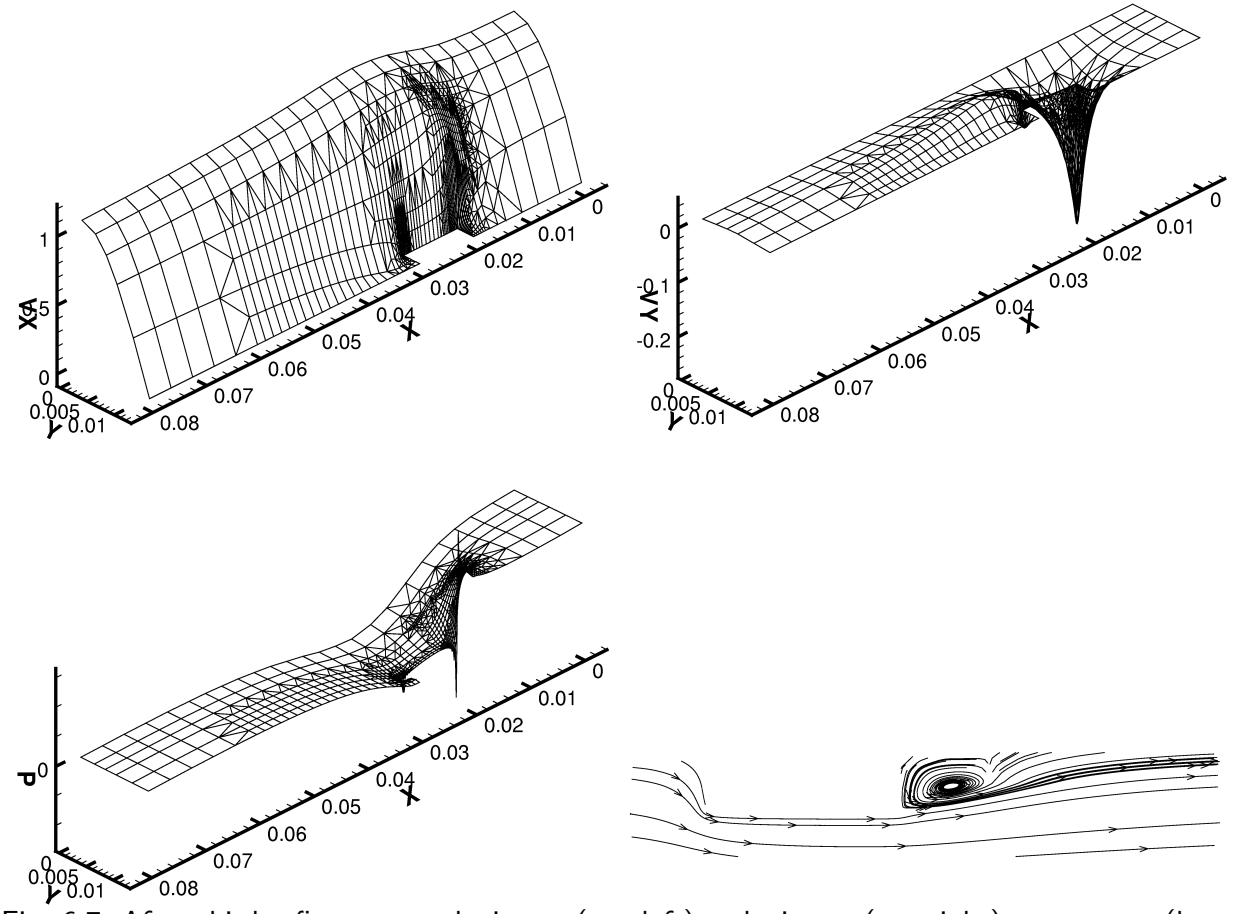

Fig. 6.7: After third refinement: velocity v_x (top left), velocity v_y (top right), pressure p (bottom left), streamlines near the corners (bottom rite)

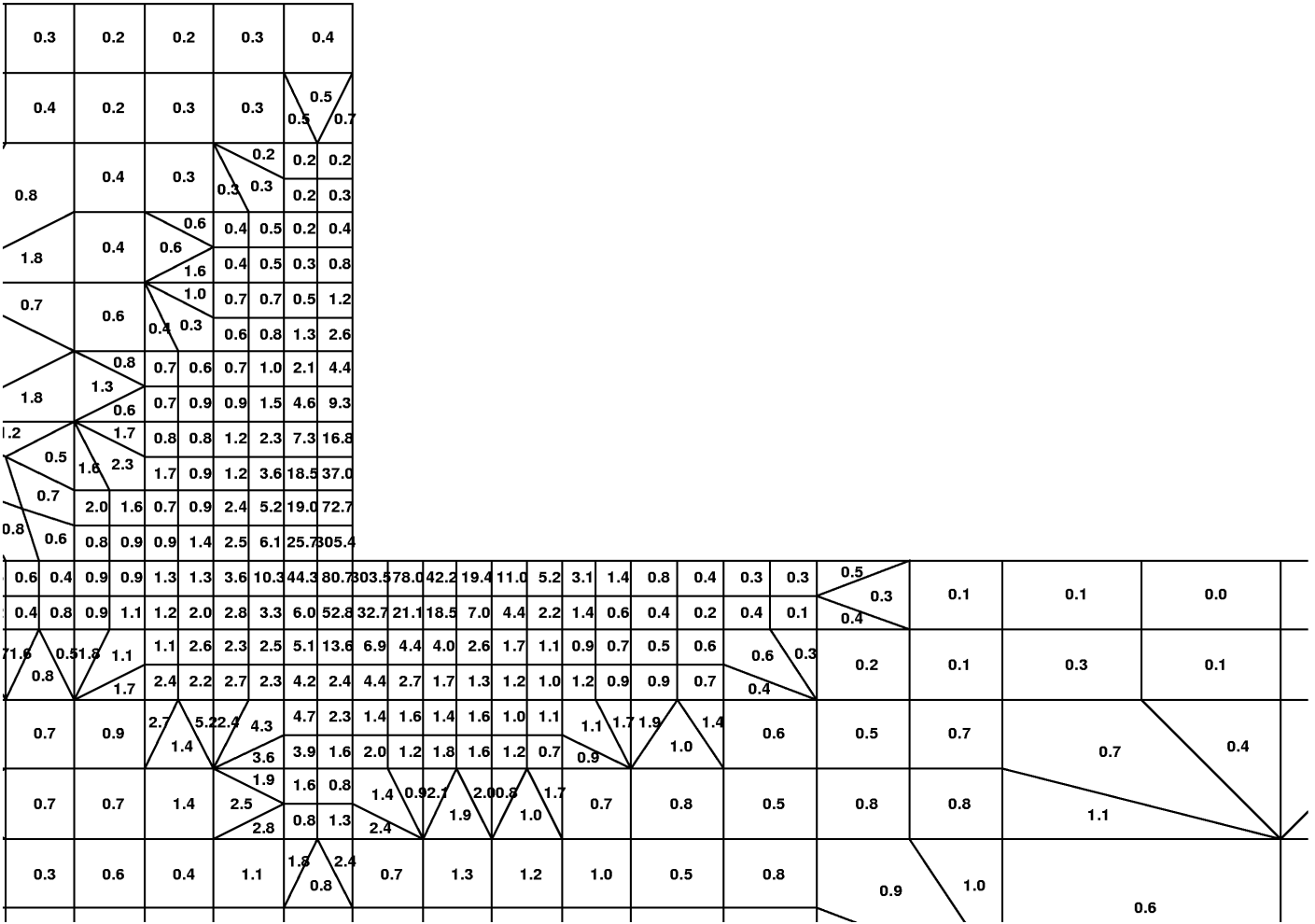

Fig. 6.8: Relative errors on elements of the third refinement

7. Application of a priori error estimates for Navier-Stokes equations to very precise solution

- Incompressible viscous flow modelled by the steady Navier-Stokes equations.
- Application of theoretical results: a priori error estimates of the FEM for NSE, and asymptotic behaviour of NSE solution near corners.
- Our algorithm: generate the computational mesh in the purpose of uniform distribution of error on elements
- Goal: very precise FEM solution on domains with corner-like singularities.
- Usual way to improve accuracy of solution by the FEM: the adaptive mesh refinement based on a posteriori error estimates or error estimators. But: could be quite time demanding, since it needs several runs of solution.
- Completely different method is applied in this chapter. Computational mesh is prepared before the first run of the solution.
- Numerical results are presented for flows in a channel with sharp obstacle and in a channel with sharp extension.

7.1. Algorithm for generation of computational mesh

Two main 'tools': The first is a priori estimate of the finite element error (cf. [18]):

$$\|\nabla(\mathbf{u}-\mathbf{u_h})\|_{L_2(\Omega)} \le C\left[\left(\sum_K h_K^{2k} \mid \mathbf{u} \mid^2_{H^{k+1}(T_K)}\right)^{1/2} + \left(\sum_K h_K^{2k} \mid p \mid^2_{H^{k}(T_K)}\right)^{1/2}\right] \quad (7.1)$$

$$\|p-p_h\|_{L_2(\Omega)} \le C\left[\left(\sum_K h_K^{2k} \mid \mathbf{u} \mid^2_{H^{k+1}(T_K)}\right)^{1/2} + \left(\sum_K h_K^{2k} \mid p \mid^2_{H^{k}(T_K)}\right)^{1/2}\right] \quad (7.2)$$

where h_K is the diameter of triangle T_K, and $k=2$ for Hood-Taylor elements.

The second tool is the asymptotic behaviour of the solution near the singularity. By (5.21), for the angle $\alpha = \frac{3}{2}\pi$, the leading term of expansion for each velocity component is

$$u_i(\rho,\vartheta) = \rho^{0.5445}\varphi_i(\vartheta) + \ldots, \; i=1,2 \quad (7.3)$$

where ρ is the distance from the corner, ϑ the angle and φ_i is a smooth function. The same expansion in the plane flow (cf. [23]), and also for the Navier-Stokes equations. Differentiating by ρ, we observe $\frac{\partial u_i(\rho,\vartheta)}{\partial \rho} \to \infty$ for $\rho \to 0$.

Taking the expansion (7.3), we can estimate

$$\mid \mathbf{u} \mid^2_{H^{k+1}(T_K)} \approx C \int_{r_K-h_K}^{r_K} \rho^{2(\gamma-k-1)}\, \rho \, d\rho = C\left[-r_K^{2(\gamma-k)} + (r_K-h_K)^{2(\gamma-k)}\right] \quad (7.4)$$

where r_K is the distance of element T_K from the corner, cf. Fig. 7.1.

Putting estimate (7.4) into the a priori estimate (7.1) or (7.2), we derive that we should guarantee

$$h_K^{2k}\left[-r_K^{2(\gamma-k)} + (r_K-h_K)^{2(\gamma-k)}\right] \approx h_{ref}^{2k} \quad (7.5)$$

in order to get the error estimate of order $O(h_{ref}^k)$ uniformly distributed on elements.

From this expression, we compute element diameters using the Newton method in accordance to chosen h_{ref}.

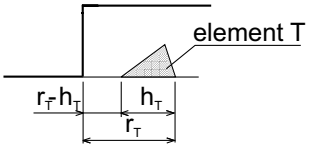

Fig. 7.1: Description of element variables

Geometry and design of the mesh

Algorithm applied to two different computational domains in 2D. The first is the channel with sudden intake of diameter (Fig. 7.2 - left), the second is the channel with abruptly extended diameter (Fig. 7.2 - right). Due to symmetry, the problem solved only on the upper half of the channels.

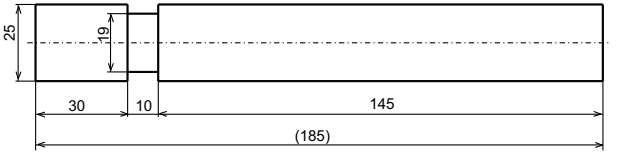

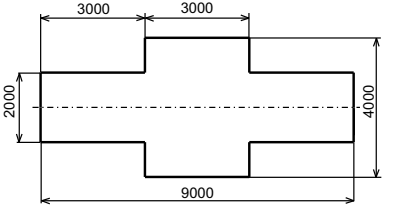

Fig. 7.2: The first geometry (left), the second geometry(right)

In the first case, diameters of elements computed for values $h_{ref} = 0.1732$ mm, $k = 2$, $\gamma = 0.5444837$. Starting distance $r_1 = 0.25$ mm from the corner.

This corresponds to cca 3% of relative error on elements. Fourteen diameters of elements obtained (see Table 7.1(left)).

For the second channel, we used $h_{ref} = 0.1732$ m, $k = 2$, $\gamma = 0.5444837$ and started in the distance $r_1 = 300$ mm from the corner. Fifteen diameters of elements were obtained (see Table 7.1(right)).

i	r_i (mm)	h_i (mm)
1	0.25000	0.06004
2	0.18996	0.04808
3	0.14189	0.03795
4	0.10394	0.02947
5	0.07447	0.02245
6	0.05202	0.01674
7	0.03527	0.01217
8	0.02311	0.00858
9	0.01453	0.00584
10	0.00869	0.00380
11	0.00489	0.00234
12	0.00255	0.00134
13	0.00121	0.00070
14	0.00050	0.00050

i	r_i (m)	h_i (m)
1	0.30000	0.06956
2	0.23044	0.05621
3	0.17423	0.04483
4	0.12940	0.03522
5	0.09419	0.02720
6	0.06699	0.02059
7	0.04640	0.01524
8	0.03116	0.01098
9	0.02017	0.00767
10	0.01250	0.00515
11	0.00735	0.00330
12	0.00405	0.00199
13	0.00206	0.00112
14	0.00094	0.00057
15	0.00038	0.00038

Table 7.1: Resulting refinement for the first (left) and the second (right) cases of geometry

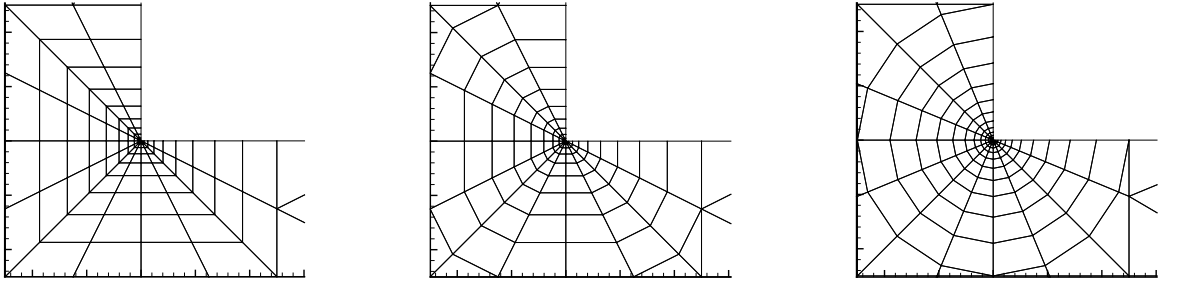

Fig. 7.3: Details of refined mesh - type A (left), type B (middle), type C (right)

The refined detail is connected to the rest of the coarse mesh. In Figures 7.4-7.5, final meshes after the refinement are shown for both geometries.

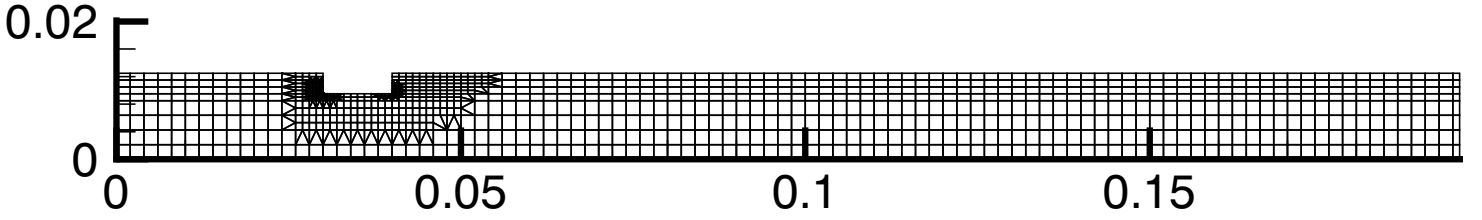

Fig. 7.4: Final computational mesh for the first channel

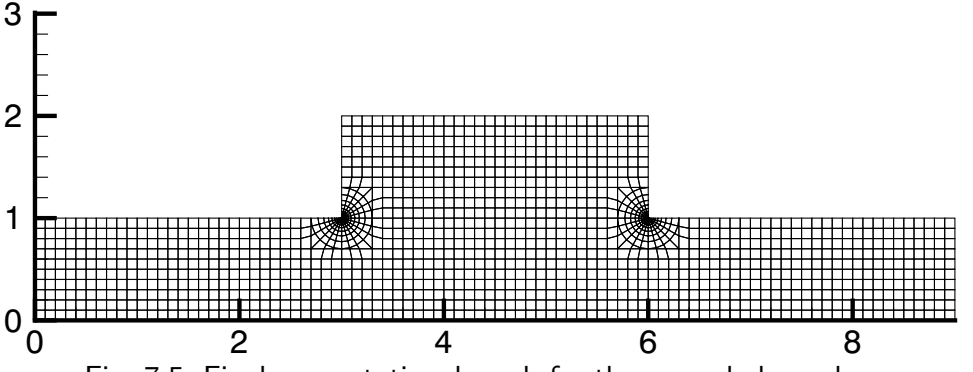

Fig. 7.5: Final computational mesh for the second channel

Measuring of error

To review the efficiency of the algorithm, we use a posteriori error estimates (6.8) as derived in Chapter 5, to evaluate the obtained error on elements. Suppose that the exact solution of the problem is denoted as (u_1, u_2, p) and the approximate solution obtained by the FEM as (u_1^h, u_2^h, p^h). The exact solution differs from the approximate solution in the error $(e_{u_1}, e_{u_2}, e_p) = (u_1 - u_1^h, u_2 - u_2^h, p - p^h)$.

In adaptive mesh refinement in Sections 5.3 - 5.5 we used the error estimator (6.14):

$$\mathcal{R}^2(u_{1h}, u_{2h}, p_h, T_K) = \frac{|\Omega|\ \mathcal{E}^2(u_{1h}, u_{2h}, p_h, T_K)}{|T_K|\ \mathcal{U}^2(u_{1h}, u_{2h}, p_h, \Omega)} \tag{7.6}$$

In this Chapter, for the similarity with a priori error estimate, we use the modified absolute error defined as

$$\mathcal{A}_m^2(u_{1h}, u_{2h}, p_h, T_K, \Omega, n) = \frac{|\Omega|\mathcal{E}^2(u_{1h}, u_{2h}, p_h, T_K)}{|\overline{T_K}|\ \mathcal{U}^2(u_{1h}, u_{2h}, p_h, \Omega)} \tag{7.7}$$

where $|\overline{T_K}|$ is the mean area of elements obtained as $|\overline{T_K}| = \frac{|\Omega|}{n}$, where n denotes the number of all elements in the domain, and the symbols $\mathcal{E}^2(u_{1h}, u_{2h}, p_h, T_K)$, $\mathcal{U}^2(u_{1h}, u_{2h}, p_h, \Omega)$ are dfefined in (6.7), (6.13).

7.2. Numerical results

Channel with sudden intake of diameter (results for Re = 1000)

In Figures 7.6-7.7, plots of entities that characterize the flow in the channel are presented. In Fig. 7.6, there are streamlines and plot of velocity component u_x. Plots of velocity component u_y and pressure are shown in Figure 7.7. Note, that the fluid flows from the right to the left on plots of u_x, u_y, and p, to have better view.

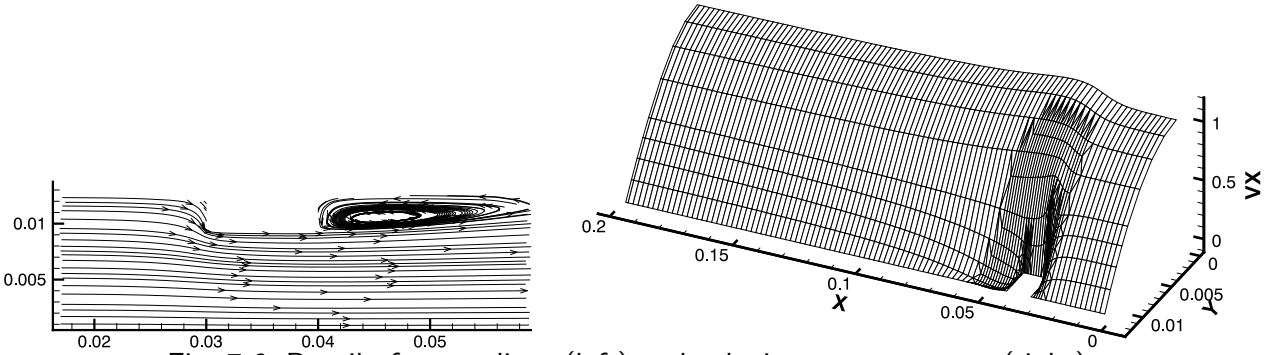

Fig. 7.6: Detail of streamlines (left) and velocity component u_x (right)

In Figure 7.9, there are values of obtained error on elements in refined area. All values are listed in Table 7.2. Marking of elements in the table is described in Figure 7.8, together with plot of contours of velocity u_y close to the corner.

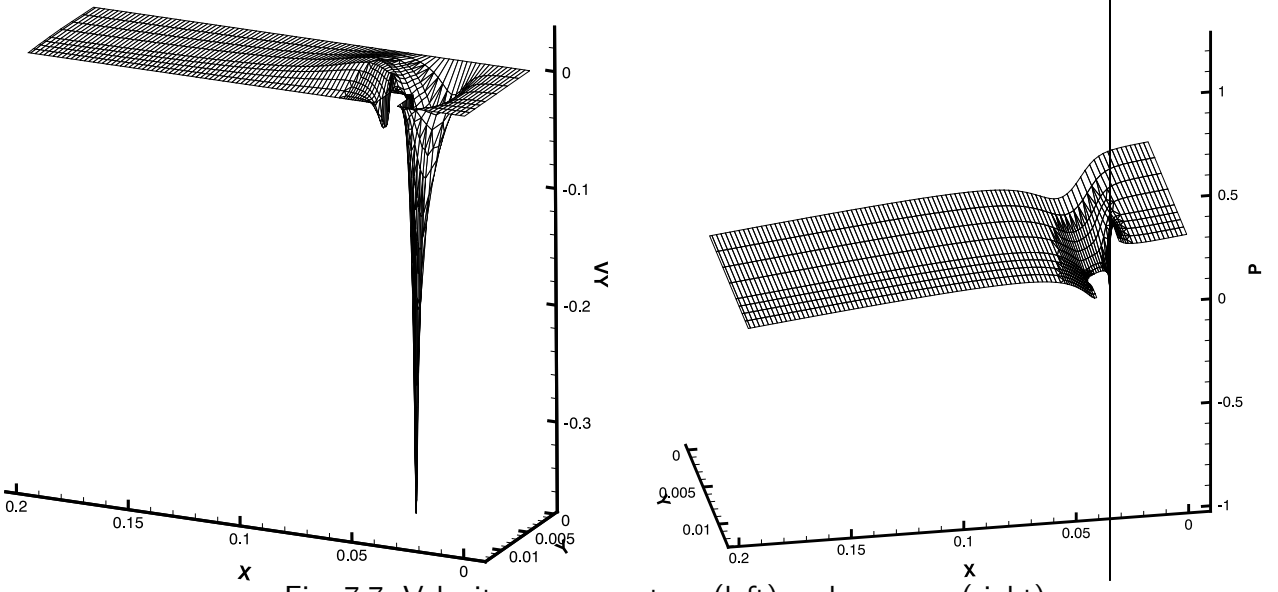

Fig. 7.7: Velocity component u_y (left) and pressure (right)

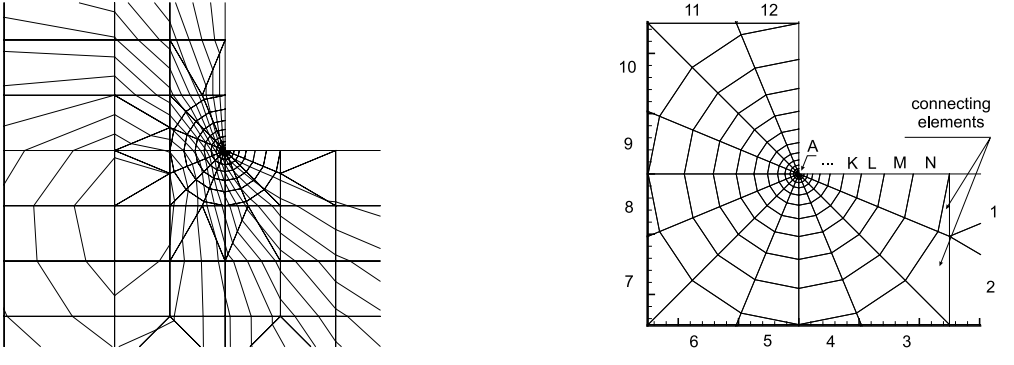

Fig. 7.8: Contours of u_y (left) and marking of elements for Tables 7.2 and **??** (right)

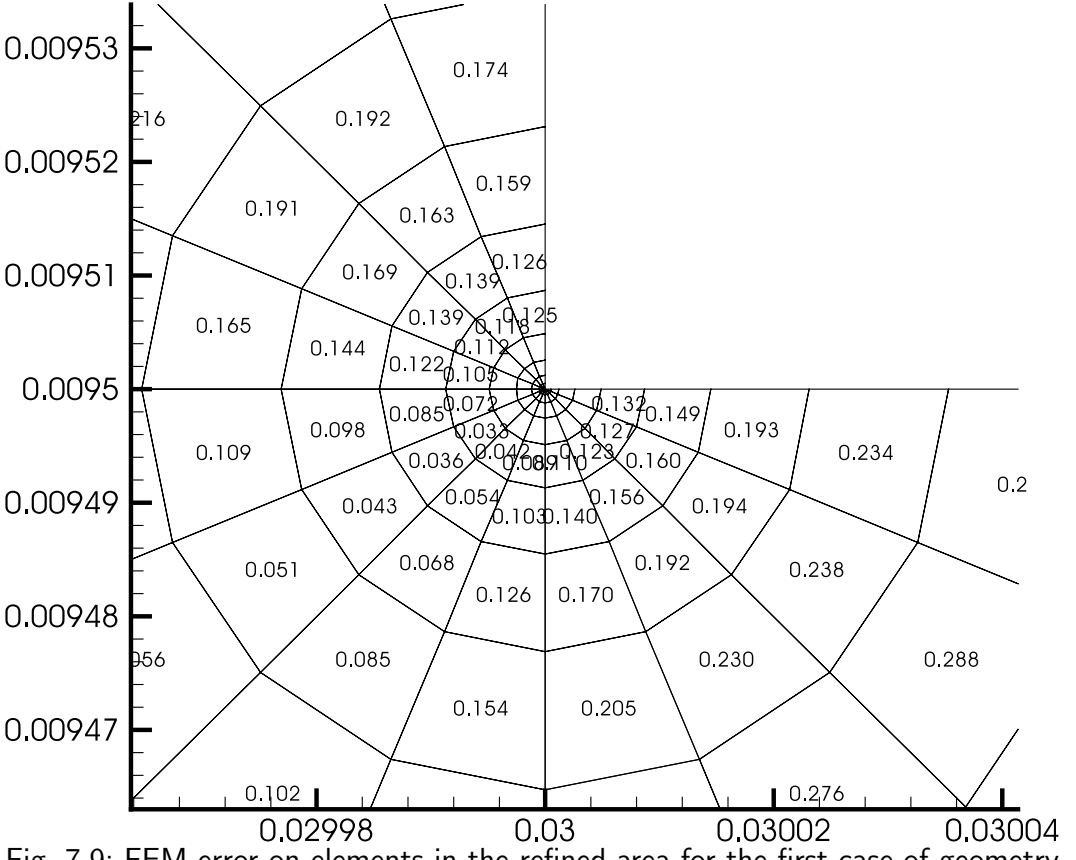

Fig. 7.9: FEM error on elements in the refined area for the first case of geometry

	A	B	C	D	E	F	G	H
1	1.858	0.652	0.229	0.103	0.132	0.149	0.193	0.234
2	2.221	0.664	0.135	0.105	0.127	0.160	0.194	0.238
3	2.427	0.513	0.122	0.103	0.123	0.156	0.192	0.230
4	2.292	0.407	0.110	0.095	0.110	0.140	0.170	0.205
5	1.574	0.261	0.083	0.069	0.087	0.103	0.126	0.154
6	0.523	0.104	0.034	0.037	0.042	0.054	0.068	0.085
7	0.585	0.093	0.032	0.030	0.033	0.036	0.043	0.051
8	1.544	0.274	0.079	0.064	0.072	0.085	0.098	0.109
9	2.223	0.404	0.115	0.091	0.105	0.122	0.144	0.165
10	2.409	0.521	0.126	0.098	0.112	0.139	0.169	0.191
11	2.277	0.654	0.134	0.101	0.118	0.139	0.163	0.192
12	1.912	0.665	0.237	0.102	0.125	0.126	0.159	0.174

	I	J	K	L	M	N	con.	-
1	0.283	0.345	0.399	0.499	0.530	0.793	1.222	-
2	0.288	0.341	0.408	0.482	0.596	0.782	1.380	-
3	0.276	0.329	0.392	0.476	0.570	1.353	2.495	-
4	0.245	0.289	0.343	0.390	0.471	0.577	1.996	-
5	0.185	0.216	0.242	0.252	0.222	0.499	1.754	-
6	0.102	0.120	0.122	0.142	0.151	0.419	1.813	-
7	0.056	0.066	0.082	0.126	0.388	1.070	3.776	-
8	0.124	0.140	0.168	0.194	0.363	0.896	1.733	-
9	0.189	0.215	0.243	0.268	0.309	0.488	0.957	-
10	0.216	0.245	0.265	0.285	0.277	0.610	1.558	-
11	0.212	0.237	0.237	0.284	0.411	1.021	2.786	-
12	0.199	0.186	0.209	0.172	0.311	0.496	1.970	-

Table 7.2: Obtained errors on elements for the first case of geometry

Channel with abruptly extended diameter (results for Re = 400)

Similarly, streamlines, plots of velocity components u_x and u_y, and pressure are presented in Figures 7.10-7.11.

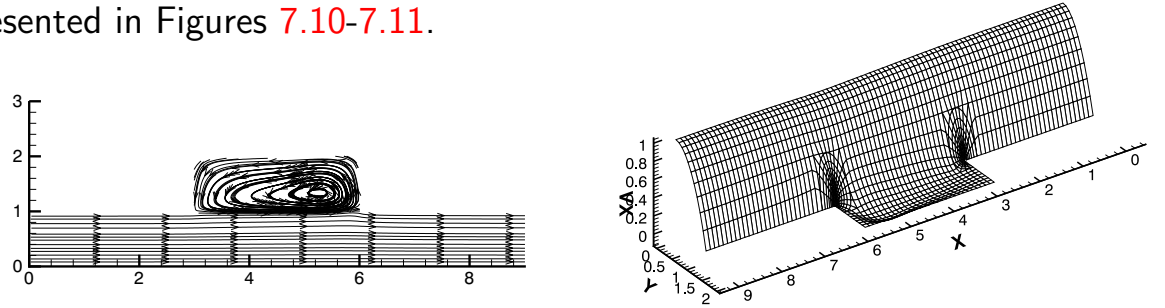

Fig. 7.10: Streamlines (left) and velocity component u_x (right)

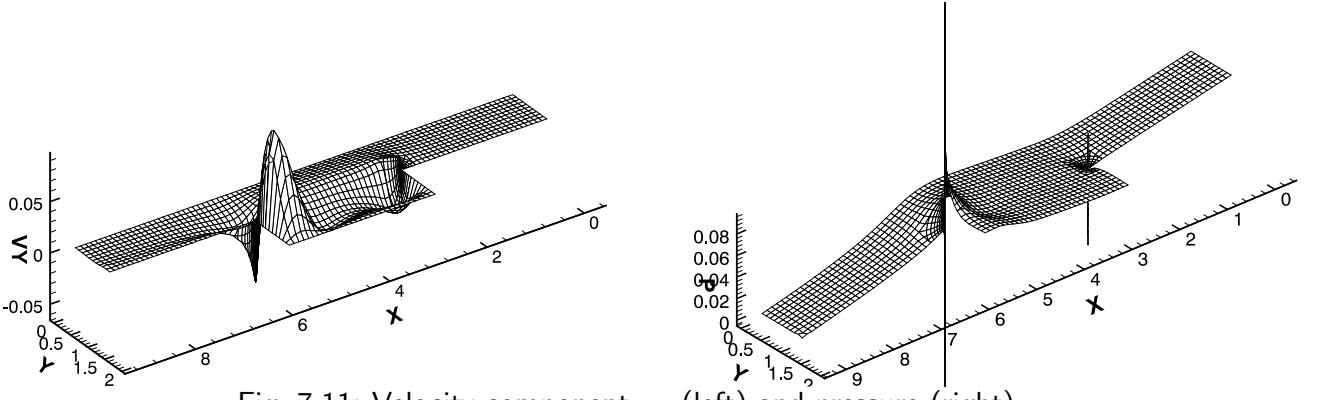

Fig. 7.11: Velocity component u_y (left) and pressure (right)

8. Numerical solution of flow problems by stabilized FEM

Motivation and goals of stabilization of FEM

- Solution of flows of incompressible viscous fluid with higher Reynolds numbers by FEM
- Stabilization techniques for FEM, Galerkin Least Squares method
- Development and implementation of an algorithm of stabilized method (semi-GLS)
- Numerical experiments
- Check of accuracy by a posteriori error estimates

8.1. Galerkin Least Squares stabilization technique

Basic scheme (Hughes, Franca, Hulbert, 1989 [[21]]).
Extension to the Navier-Stokes equations (Franca, Madureira, 1993 [17]]):
For system

$$\begin{aligned}(\nabla\mathbf{u})\mathbf{u} - 2\nu\nabla\cdot\varepsilon(\mathbf{u}) + \nabla p &= \mathbf{f} \quad \text{in } \Omega \\ \nabla\cdot\mathbf{u} &= 0 \quad \text{in } \Omega \\ \mathbf{u} &= \mathbf{0} \quad \text{on } \Gamma \\ \varepsilon(\mathbf{u})_{ij} &= \frac{1}{2}\left(\frac{\partial u_i}{\partial x_j} + \frac{\partial u_j}{\partial x_i}\right)\end{aligned}$$

introduce stabilized problem

- *Find* $\mathbf{u}_h \in V_{gh}$ *and* $p_h \in Q_h$ *satisfying in* Ω

$$B_{GLS}(\mathbf{u}_h, p_h; \mathbf{v}_h, \psi_h) = L_{GLS}(\mathbf{v}_h, \psi_h), \quad \forall \mathbf{v}_h \in V_h, \quad \forall \psi_h \in Q_h$$

where

$$\begin{aligned} & B_{GLS}(\mathbf{u}_h, p_h; \mathbf{v}_h, \psi_h) \equiv \\ \equiv\ & ((\mathbf{u}_h\cdot\nabla)\mathbf{u}_h, \mathbf{v}_h)_0 + (2\nu\varepsilon(\mathbf{u}_h), \varepsilon(\mathbf{v}_h))_0 - (p_h, \nabla\cdot\mathbf{v}_h)_0 + \\ +\ & (\psi_h, \nabla\cdot\mathbf{u}_h)_0 + (\nabla\cdot\mathbf{u}_h, \delta\nabla\cdot\mathbf{v}_h)_0 + \\ +\ & \sum_K \left((\mathbf{u}_h\cdot\nabla)\mathbf{u}_h + \nabla p_h - 2\nu\nabla\cdot\varepsilon(\mathbf{u}_h), \tau((\mathbf{u}_h\cdot\nabla)\mathbf{v}_h + \nabla\psi_h - 2\nu\nabla\cdot\varepsilon(\mathbf{v}_h))\right)_{T_K} \\ & L_{GLS}(\mathbf{v}_h, \psi_h) \equiv (\mathbf{f}, \mathbf{v}_h)_0 + \sum_K \left(\mathbf{f}, \tau((\mathbf{u}_h\cdot\nabla)\mathbf{v}_h + \nabla\psi_h - 2\nu\nabla\cdot\varepsilon(\mathbf{v}_h))\right)_{T_K}\end{aligned}$$

Our implementation

- we do not consider stabilization of the continuity equation ($\delta = 0$). For this reason, we call the technique *semiGLS* (abbreviated *sGLS*).
- we use formulation with Laplacian instead of $\varepsilon(\mathbf{u})_{ij}$

Find $\mathbf{u}_h(t) \in V_{gh},\ t \in [0,T]$ *and* $p_h(t) \in Q_h,\ t \in [0,T]$ *satisfying for any* $t \in [0,T]$

$$B_{sGLS}(\mathbf{u}_h, p_h; \mathbf{v}_h, \psi_h) = L_{sGLS}(\mathbf{v}_h, \psi_h), \quad \forall \mathbf{v}_h \in V_h, \quad \forall \psi_h \in Q_h$$

where

$$B_{sGLS}(\mathbf{u}_h, p_h; \mathbf{v}_h, \psi_h) \equiv \int_\Omega \frac{\partial \mathbf{u}_h}{\partial t} \cdot \mathbf{v}_h \mathrm{d}\Omega + \int_\Omega (\mathbf{u}_h \cdot \nabla)\mathbf{u}_h \cdot \mathbf{v}_h \mathrm{d}\Omega$$
$$+ \ \nu \int_\Omega \nabla \mathbf{u}_h : \nabla \mathbf{v}_h \mathrm{d}\Omega - \int_\Omega p_h \nabla \cdot \mathbf{v}_h \mathrm{d}\Omega + \int_\Omega \psi_h \nabla \cdot \mathbf{u}_h \mathrm{d}\Omega +$$
$$+ \ \sum_{K=1}^{N} \int_{T_K} \left[\frac{\partial \mathbf{u}_h}{\partial t} + (\mathbf{u}_h \cdot \nabla)\mathbf{u}_h - \nu \Delta \mathbf{u}_h + \nabla p_h \right] \cdot \tau \left[(\mathbf{u}_h \cdot \nabla)\mathbf{v}_h - \nu \Delta \mathbf{v}_h + \nabla \psi_h \right] \mathrm{d}\Omega$$

$$L_{sGLS}(\mathbf{v}_h, \psi_h) \ \equiv \ \int_\Omega \mathbf{f} \cdot \mathbf{v}_h \mathrm{d}\Omega + \sum_{K=1}^{N} \int_{T_K} \mathbf{f} \cdot \tau \left[(\mathbf{u}_h \cdot \nabla)\mathbf{v}_h - \nu \Delta \mathbf{v}_h + \nabla \psi_h \right] \mathrm{d}\Omega$$

8.2. Results of numerical experiments

Test problems:

- lid driven cavity – steady
- channel with sudden extension of diameter – steady
- flow past NACA 0012 airfoil – unsteady

The effect of stabilization: the difference of solutions obtained with and without stabilization:

$$\delta_\eta = \sqrt{\frac{\sum_{i=1}^{n}(\eta_{sGLS_i} - \eta_{Newton_i})^2}{\sum_{i=1}^{n}\eta_{Newton_i}^2}} \cdot 100 \quad [\%] \tag{8.1}$$

where η means in turn u_{h1}, u_{h2} and p_h, n denotes number of nodes with η given, η_{sGLS} denotes the solution by the semiGLS algorithm and η_{Newton} the solution by the Newton method without stabilization. Results summarized in Table 8.1.

Differences of solutions obtained by the semiGLS method from those obtained by the Newton method computed by (8.1) are big for the problem of cavity.

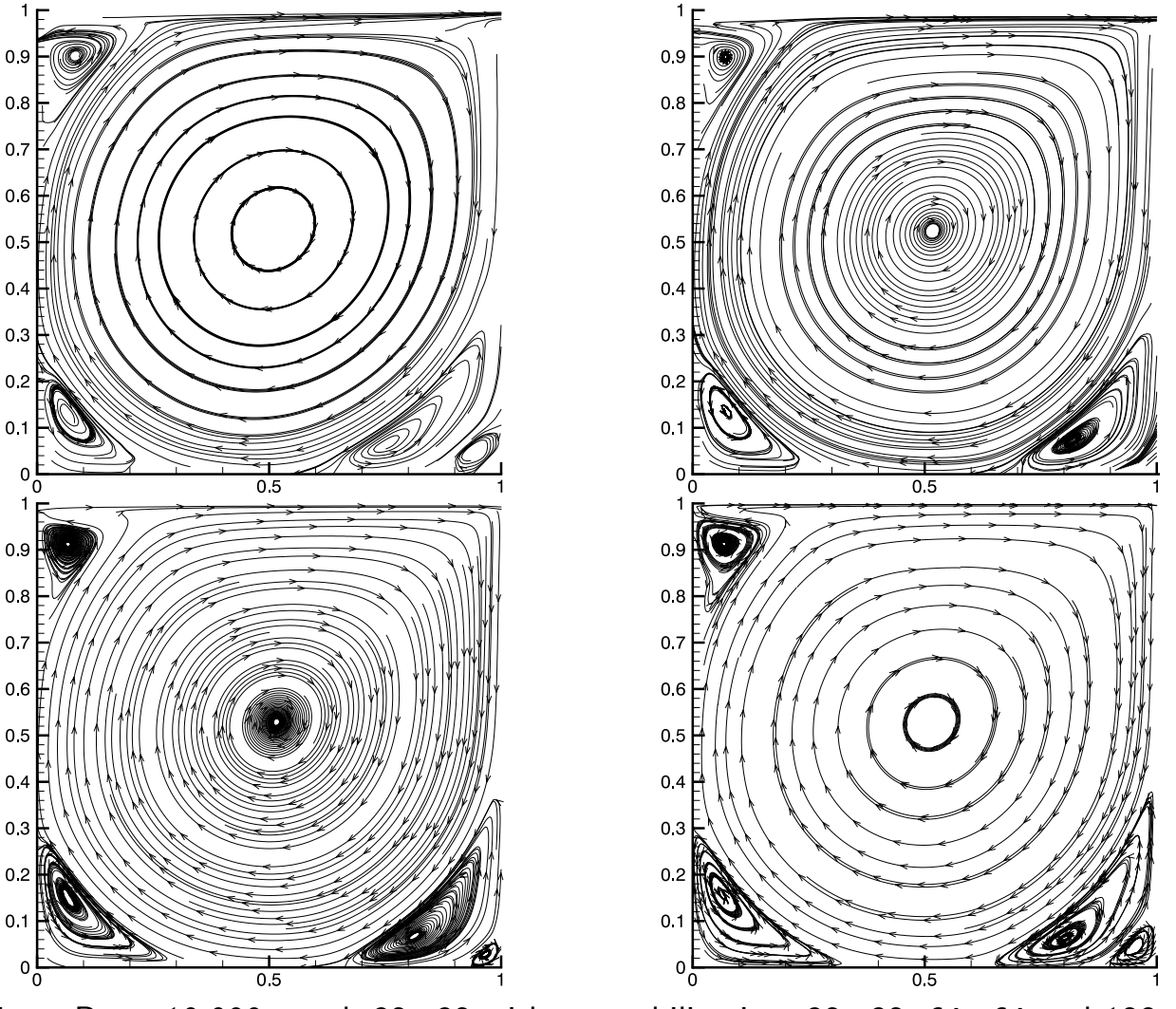

Streamlines, Re = 10,000, mesh 32×32 without stabilization, 32×32, 64×64 and 128×128

mesh	32×32	64×64	128×128
$\delta_{u_{h1}}$ [%]	41.69	39.07	21.42
$\delta_{u_{h2}}$ [%]	70.81	49.12	22.24
δ_{p_h} [%]	197.90	137.10	42.82

Table 8.1: Differences between solutions obtained with and without stabilization

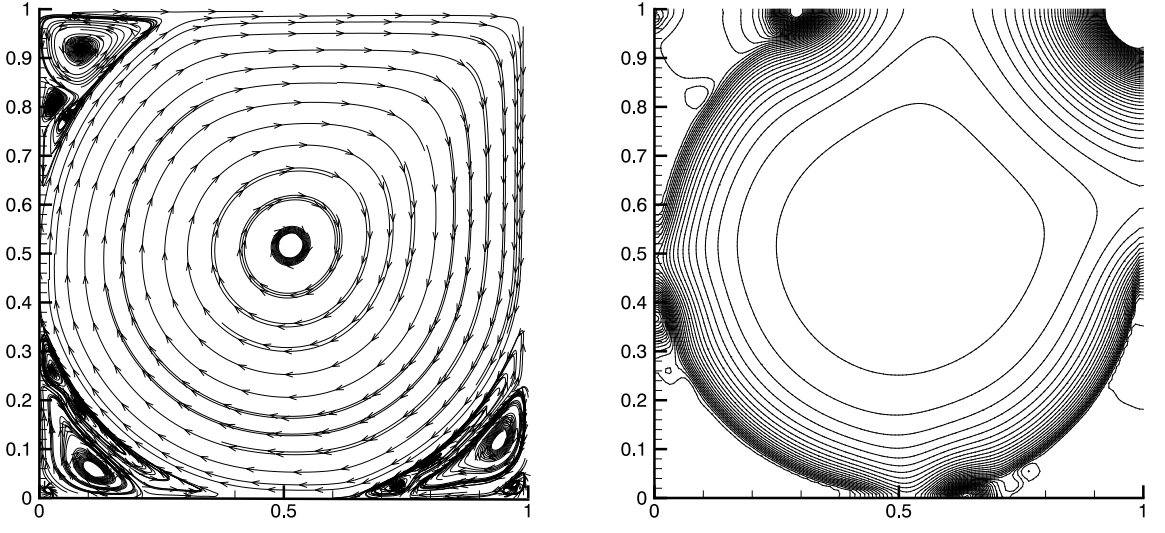

Streamlines and pressure contours for Re = 100,000, mesh 128×128

CHANNEL WITH SUDDEN EXTENSION OF DIAMETER - STEADY FLOW

Steady flow in 2D channel with abruptly extended diameter (Figure 8.1). Complicated due to singularities of solution in the vicinity of nonconvex internal corners. The aspect of suitable mesh generation studied in [10] and [27]. We compare solutions with and without semiGLS stabilization. Streamlines presented in Figure 8.2 for Reynolds number 1,000. Differences between solutions computed by (8.1) listed in Table 8.2.

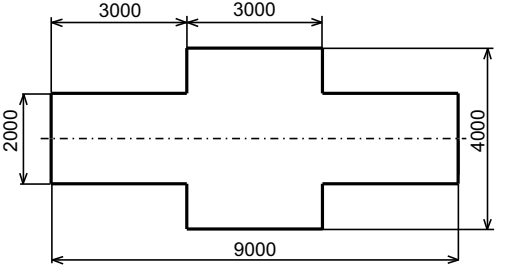

Fig. 8.1: Geometry of the channel

mesh	channel (Figure 8.1)
$\delta_{u_{h1}}$ [%]	0.0718
$\delta_{u_{h2}}$ [%]	2.7202
δ_{p_h} [%]	0.5139

Table 8.2: Differences between solutions obtained with and without stabilization

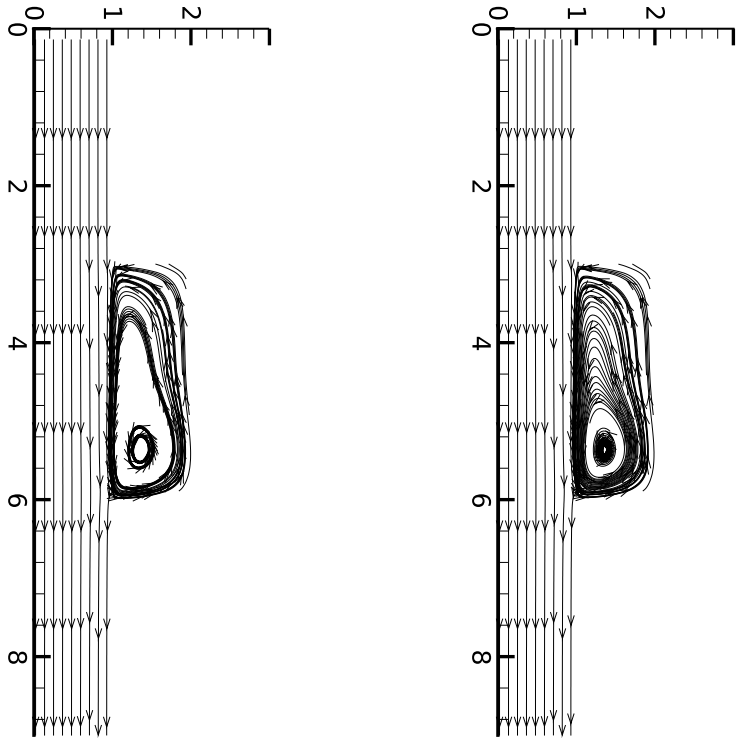

Fig. 8.2: Streamlines in the channel by the Newton method without stabilization (left) and streamlines by the semiGLS algorithm (right), Re = 1,000

Additionally, we present streamlines, plots of velocities and pressure for Reynolds number 80,000 in Figure 8.3.

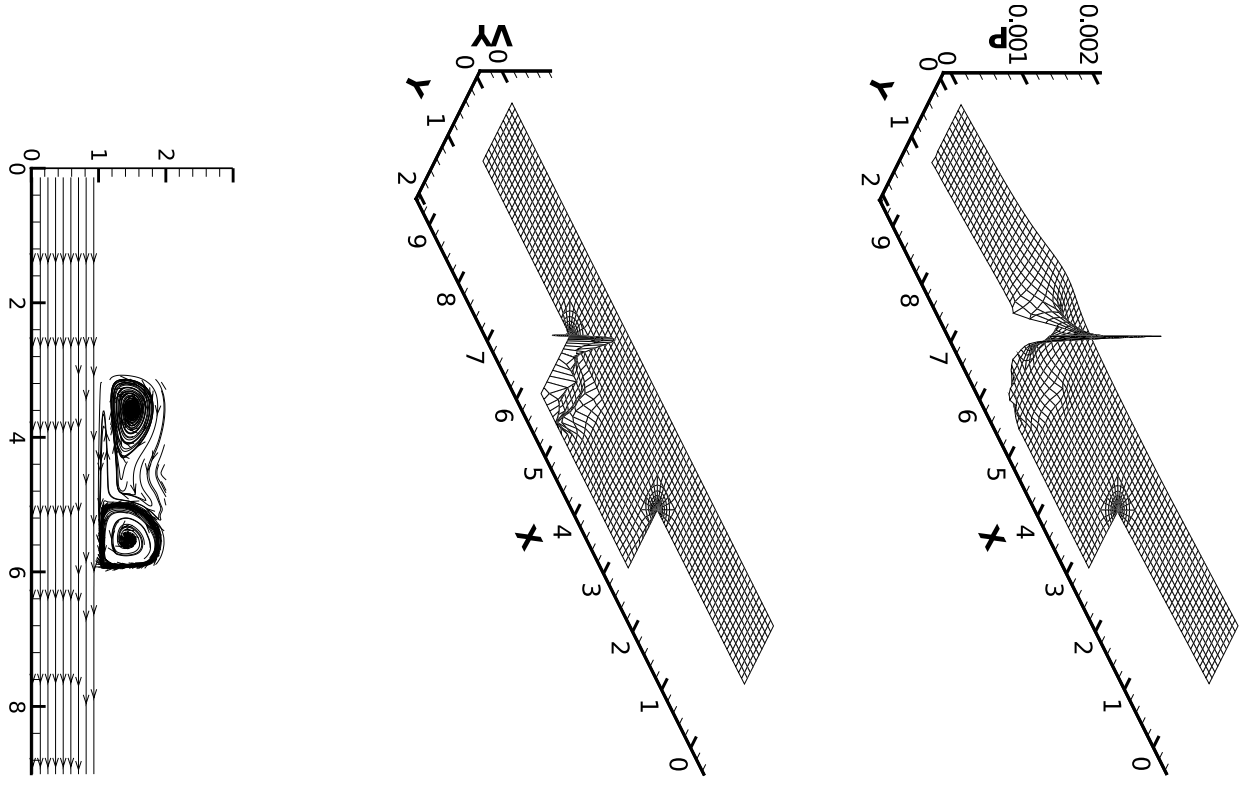

Fig. 8.3: Streamlines (left), plot of velocity u_{h2} (center) and pressure (right) by the semiGLS algorithm, Re = 80,000

UNSTEADY SOLUTION OF FLOW PAST NACA 0012 AIRFOIL

Results for angle of incidence of 34° and Re = 1,000 by unconditionaly stable projection FEM (Guermond and Quartapelle [20]) compared in Figures 8.5-8.8, to ours by the semiGLS algorithm. Then streamlines and pressure contours for Re = 100,000 are presented in Figures 8.9-8.10. The mesh (see Figure 8.4) of 6,220 elements, 18,478 nodes, and 43,085 DOFs. Data: zero initial condition, unit horizontal velocity on the left part of the boundary and 'do nothing' boundary condition on the rest. Time steps for Re = 1,000 are 0.01 s and for Re = 100,000 are 0.005 s (see Šístek [27] for details).

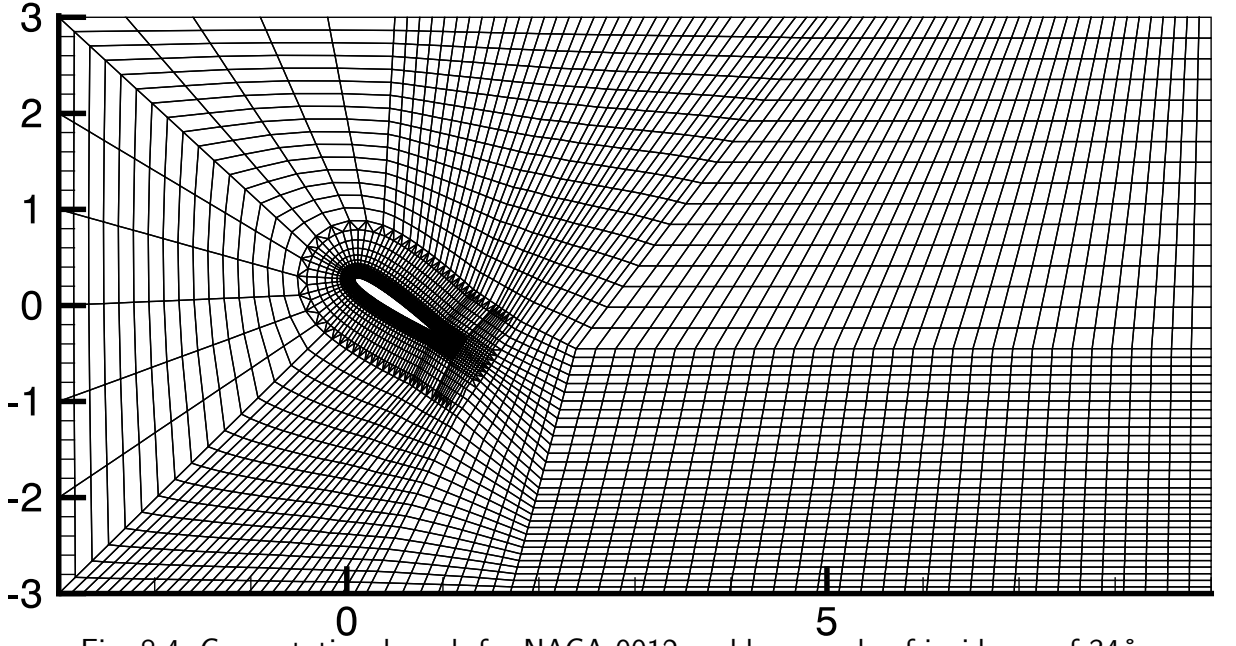

Fig. 8.4: Computational mesh for NACA 0012 problem, angle of incidence of 34°

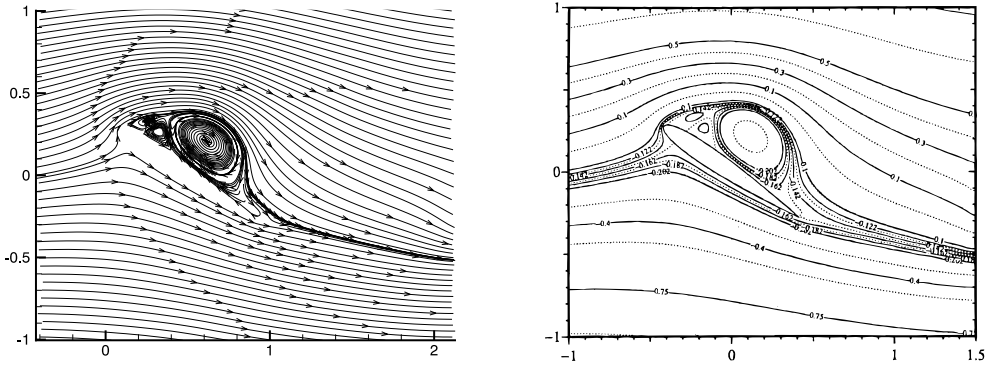

Fig. 8.5: Streamlines by the semiGLS algorithm (left) and by [20] (right), $t = 1.6s$, Re = 1,000

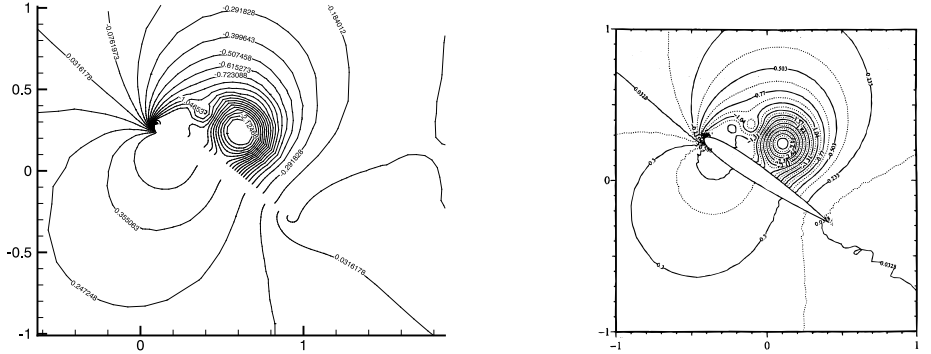

Fig. 8.6: Pressure contours by the semiGLS algorithm (left) and by [20] (right), $t = 1.6s$, Re = 1,000

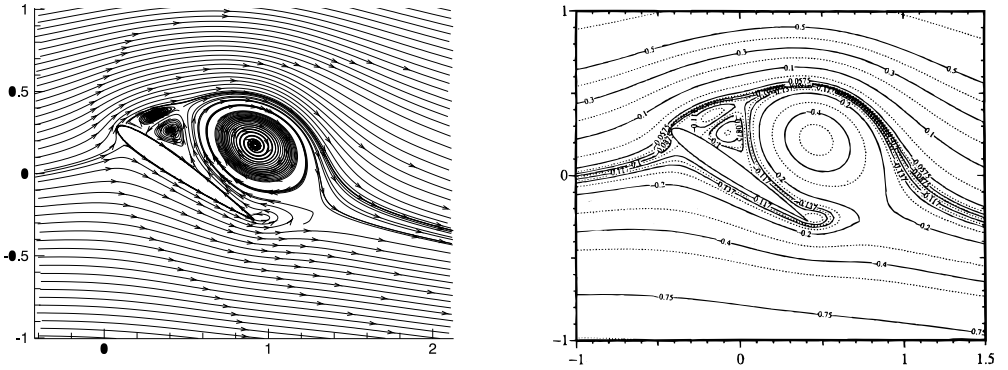

Fig. 8.7: Streamlines by the semiGLS algorithm (left) and by [20] (right), $t = 2.6s$, Re = 1,000

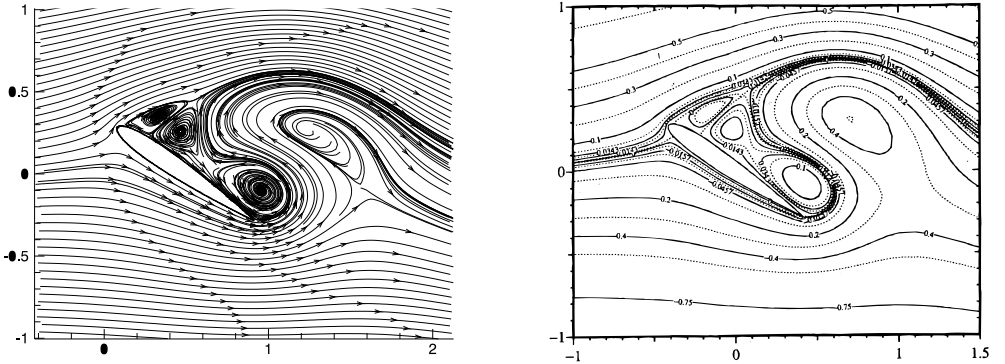

Fig. 8.8: Streamlines by the semiGLS algorithm (left) and by [20] (right), $t = 3.6s$, Re = 1,000

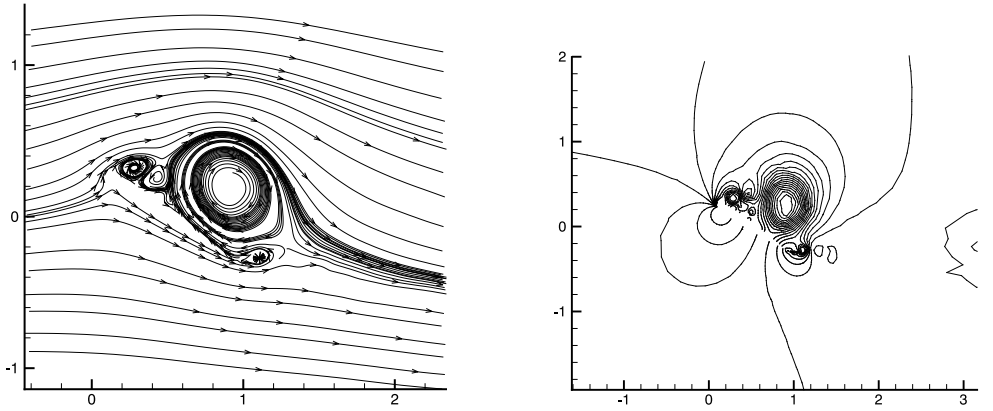

Fig. 8.9: Streamlines (left) and pressure contours (right) by the semiGLS algorithm, $t = 2.6s$, Re = 100,000

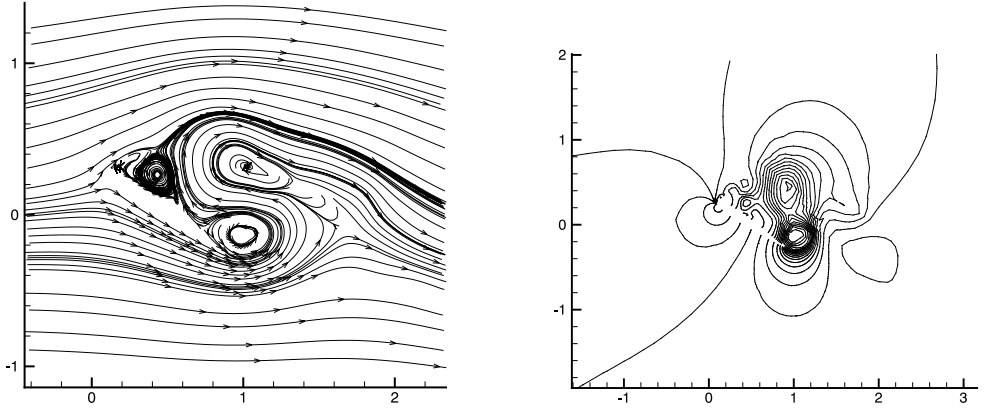

Fig. 8.10: Streamlines (left) and pressure contours (right) by the semiGLS algorithm, $t = 3.6s$, Re = 100,000

8.3. Application of a posteriori error estimates

Test problem: lid driven cavity – steady GLS

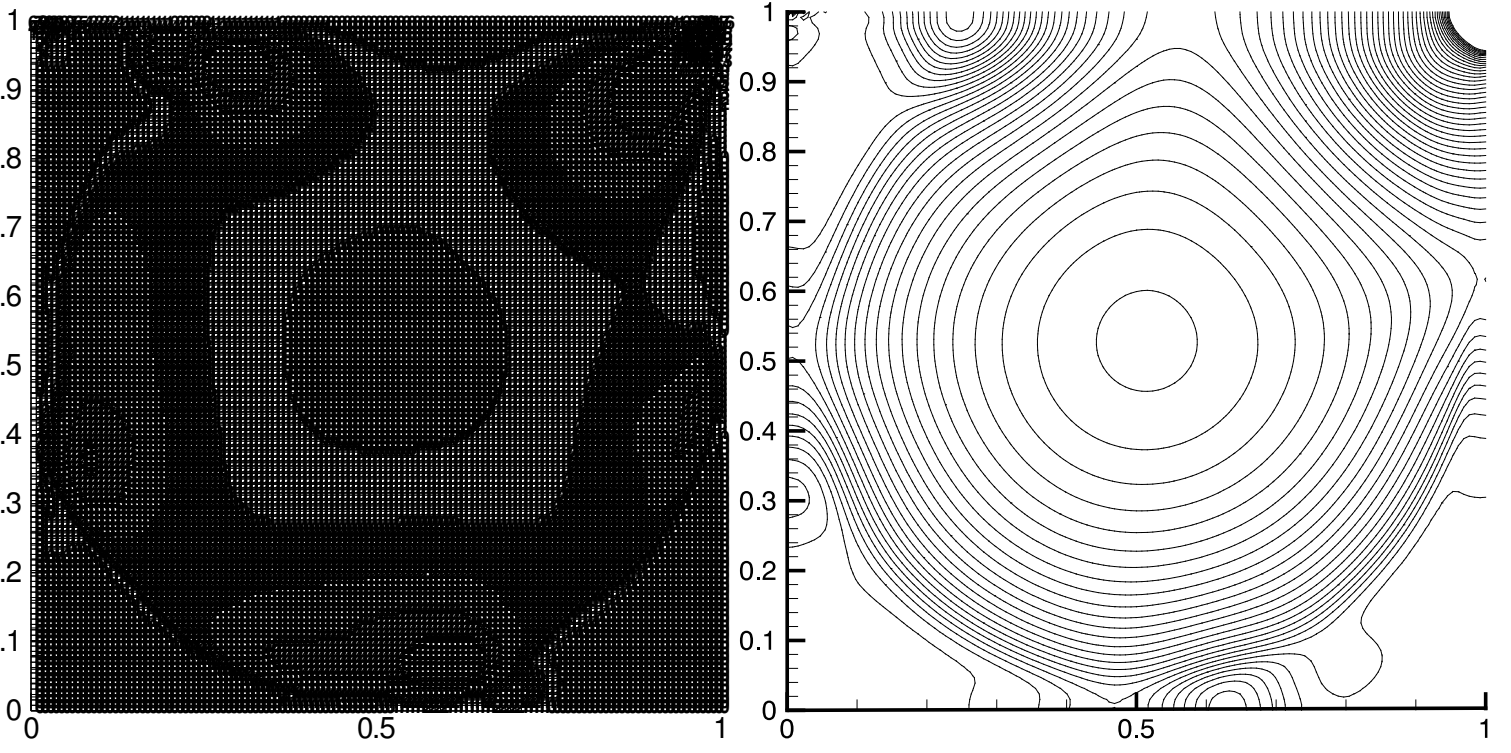

Pressure contours and errors on elements for Re = 10,000, mesh 128×128

Accuracy of stabililized FEM using a posteriori estimates:

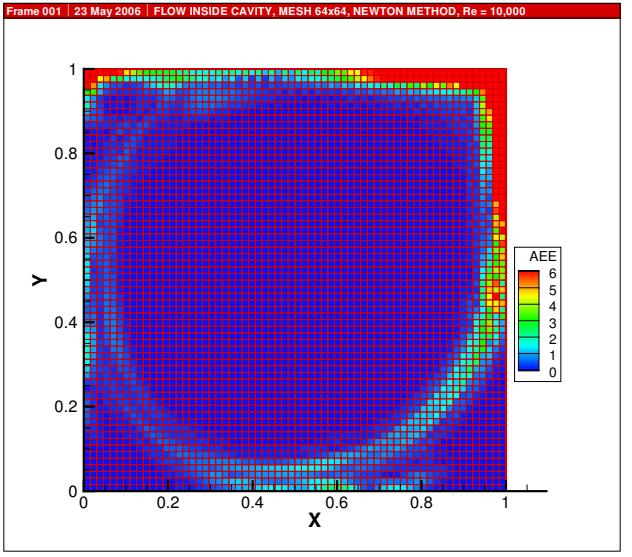

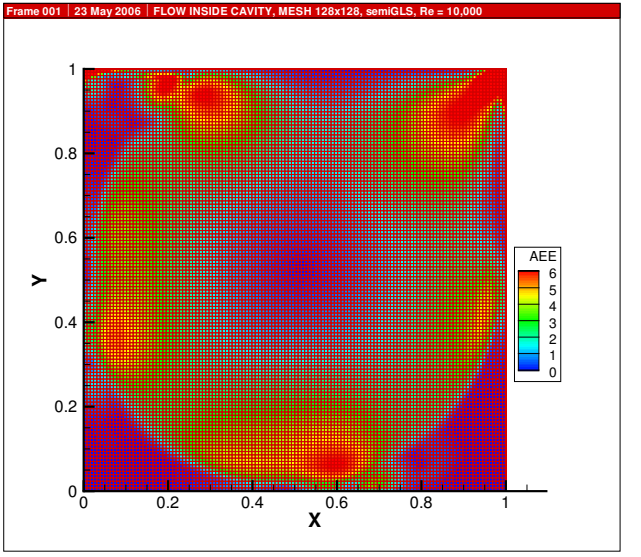

rrors on elements (Re = 10,000) left: Newton - mesh 64×64, right: semiGLS - mesh 128×128

Conclusions

- Derivation and implementation of FEM algorithm for solving flow problems
- Modification of GLS technique of stabilization
- Comprehensive testing of developed method
- We reached higher Reynolds numbers in solved problems
- For reaching higher Re – **stabilization + mesh refinement**

Future. . .

- Evaluate the distortion of solution affected by the stabilization (aposteriori error estimates for stabilized FEM)
- Implement and compare other stabilization techniques (Glowinski, Tezduyar, . . .)

9. Conclusion

- Mathematical models for incompressible flows: Navier-Stokes equations, Stokes problem.
- One focus: flow problems with singularities due to corners in the solution domain.
- Two ways to desired precision (based on qualitative properties)
- First approach (Chapter 5): use a posteriori error estimates of the FEM solution. The role of constant.
- Adaptive strategy to improve the mesh and thus the FEM solution. Numerical results demonstrate the robustness of this approach.
- The alternative way based on the asymptotic expansion of the exact solution near the corner and on the a priori error estimate of the FEM solution
- Derived an algorithm for designing the FEM mesh a priori, to get the solution with desired precision near the corners, though there is a singularity there.
- This approach saves a lot of computational time using mesh 'prepared' in advance
- Second focus: flows with higher Reynolds numbers
- Developed stabilized version of FEM [27],[11], [12].
- Combine stabilization with a posteriori estimates. Achievements on precise solution of problems with singularities - a very cheap tool for verification [13].

10. References

[1] Agmon, S., Douglis, A., Nirenberg, L., Estimates near the boundary for solutions of elliptic partial differential equations satisfying general boundary conditions. I., Comm. Pure Appl. Math. **12**, 1959, 623-727.

[2] Ainsworth, M., Oden, J., T. (1997): A posteriori error estimators for the Stokes and Oseen problems. SIAM J. Numer. Anal., **34**, 228 - 245

[3] Babuška, I., Rheinboldt, W., C. (1978): A posteriori error estimates for the finite element method. Internat. J. Numer. Meth. Engrg., **12**, 1597 - 1615

[4] Brezzi, F., Fortin, M. *Mixed and Hybrid Finite Element Methods*, Springer, Berlin, 1991

[5] Burda, P. *On the FEM for the Navier-Stokes equations in domains with corner singularities*. In: Křížek, M., et al., editors. Finite Element Methods, Marcel Dekker, New York, 1998, 41-52

[6] Burda, P. (2000): An a posteriori error estimate for the Stokes problem in a polygonal domain using Hood-Taylor elements. In: Neittaanmäki, P., Tiihonen, T., and Tarvainen, P. (eds) ENUMATH 99, Proc. of the 3-rd Europ. Conf. on Numer. Math. and Advanced Applications. World Scientific, Singapore, 448 - 455

[7] Burda, P. *A posteriori error estimates for the Stokes flow in 2D and 3D domains*. In: Neittaanmäki, P., Křížek, M., editors. Finite Element Methods, 3D.(GAKUTO Internat. Series, Math. Sci. and Appl., Vol. 15), Gakkotosho, Tokyo, 2001, 34-44

[8] Burda, P., Kořenář, J. *Numerical solution of pulsatile flow in a round tube with axisymmetric constrictions*. In: COMMUNICATIONS, Vol. 19, Institute of Hydrodynamics, Prague, 1992, 87-110

[9] Burda, P., Novotný, J., Sousedík, B. *A posteriori error estimates applied to flow in a channel with corners*, Mathematics and Computers in Simulation, **61** (2003), 375-383

[10] Burda, P., Novotný, J., Šístek, J., Precise FEM solution of corner singularity using adjusted mesh applied to axisymmetric and plane flow, ICFD Conf. Oxford, 2004, Int. J. Num. Meth. Fluids, **47**, 2005, pp. 1285 - 1292.

[11] Burda, P., Novotný, J., Šístek, J., On a modification of GLS stabilized FEM for solving incompressible viscous flows, Int. J. Numer. Meth. Fluids, **51**, 2006, 1001 - 1016.

[12] Burda, P., Novotný, J., Šístek, J., Numerical solution of flow problems by stabilized finite element method, Modelling 2005, Plzeň, July, 2005, In: Mathematics and Computers in Simulation **76** (2007), pp. 28 - 33.

[13] Burda, P., Novotný, J., Šístek, J., Accuracy of semiGLS stabilization of FEM for solving Navier-Stokes equations and a posteriori error estimates, ICFD Conference on Numerical Methods for Fluid Dynamics, Int. J. Numer. Meth. Fluids, **56**, 2008, 1167 - 1173.

[14] Damašek, A., Burda, P., Finite element modelling of viscous incompressible fluid flow in glottis, ENGENEERING MECHANICS 2003, Svratka, May 12-15, 2003, In: ENGENEERING MECHANICS (CD-ROM) Praha, Ústav termomechaniky AV ČR, 2003, 9 pp.

[15] Dauge, Monique, Stationary Stokes system in two or three dimensional domains with corners, Seminaire Equations aux Derivees Partielles 1987, expos, no. 10, Univ. de Nantes, 315-357.

[16] Eriksson, K., Estep, D., Hansbo, P., Johnson, C. (1995): Introduction to adaptive methods for differential equations. Acta Numerica,**1995**, CUP, 105–158.

[17] Franca, L., P., Madureira, A., L. *Element diameter free stability parameters for stabilized methods applied to fluids*, Comp. Meth. Appl. Mech. Eng., **105** (1993), 395-403

[18] Girault, V., Raviart, P., G. *Finite Element Method for Navier-Stokes Equations*, Springer, Berlin, 1986

[19] Glowinski, R. *Finite Element Methods for Incompressible Viscous Flow*, Handbook of Numerical Analysis, Vol. IX, Elsevier, 2003

[20] Guermond, J., L., Quartapelle, L. *Calculation of viscous incompressible viscous flow by an unconditionally stable projection FEM*, J. Comp. Phys., **132** (1997), 12-33

[21] Hughes, T., J., R., Franca, L., P., Hulbert, G., M. *A new finite element formulation for computational fluid dynamics: VIII. The Galerkin/least-squares method for advective-diffusive equations*, Comp. Meth. Appl. Mech. Eng., **73** (1989), 173-189

[22] Johnson, C. *Numerical Solution of Partial Differential Equations by the Finite Element Method*, Cambridge University Press, 1994

[23] Kondratiev, V., A. *Asimptotika rešenija uravnienija Nav'je-Stoksa v okrestnosti uglovoj točki granicy*, Prikl. Mat. i Mech., **1** (1967), 119-123

[24] Kondratiev, V. A., Krajevyje zadači dlja elliptičeskich uravněnij v oblasťach s koniěskimi i uglovymi točkami, Trudy Moskov. Mat. obshch. 16 (1967), 209 - 292.

[25] Kondratiev, V. A., Olejnik, O. A., Krajevyje zadači dlja uravněnij s častnymi proizvodnzmi v negladkich oblasťach, Uspechi Mat. Nauk 38 (1983), 3-76.

[26] Ladevéze J., Peyret, R., Calcul numérique d'une solution avec singularité des équations de Navier-Stokes: écoulement dans un canal avec variation brusque de section, Journal de Mécanique 13 (1974), 367-396.

[27] Šístek, J. *Stabilization of finite element method for solving incompressible viscous flows*, Diploma thesis, ČVUT, Praha, 2004

[28] Verfürth, R. (1996): A Review of A Posteriori Error Estimation and Adaptive Mesh-Refinement Techniques. Wiley and Teubner, Chichester